



University Transportation Research Center - Region 2

Final Report



Energy Efficient and Environmental Friendly Cement Free Concrete (CFC) for Pavement and Bridge Deck Application

Performing Organization: Clarkson University



April 2014



Sponsor:
University Transportation Research Center - Region 2

University Transportation Research Center - Region 2

The Region 2 University Transportation Research Center (UTRC) is one of ten original University Transportation Centers established in 1987 by the U.S. Congress. These Centers were established with the recognition that transportation plays a key role in the nation's economy and the quality of life of its citizens. University faculty members provide a critical link in resolving our national and regional transportation problems while training the professionals who address our transportation systems and their customers on a daily basis.

The UTRC was established in order to support research, education and the transfer of technology in the field of transportation. The theme of the Center is "Planning and Managing Regional Transportation Systems in a Changing World." Presently, under the direction of Dr. Camille Kamga, the UTRC represents USDOT Region II, including New York, New Jersey, Puerto Rico and the U.S. Virgin Islands. Functioning as a consortium of twelve major Universities throughout the region, UTRC is located at the CUNY Institute for Transportation Systems at The City College of New York, the lead institution of the consortium. The Center, through its consortium, an Agency-Industry Council and its Director and Staff, supports research, education, and technology transfer under its theme. UTRC's three main goals are:

Research

The research program objectives are (1) to develop a theme based transportation research program that is responsive to the needs of regional transportation organizations and stakeholders, and (2) to conduct that program in cooperation with the partners. The program includes both studies that are identified with research partners of projects targeted to the theme, and targeted, short-term projects. The program develops competitive proposals, which are evaluated to insure the most responsive UTRC team conducts the work. The research program is responsive to the UTRC theme: "Planning and Managing Regional Transportation Systems in a Changing World." The complex transportation system of transit and infrastructure, and the rapidly changing environment impacts the nation's largest city and metropolitan area. The New York/New Jersey Metropolitan has over 19 million people, 600,000 businesses and 9 million workers. The Region's intermodal and multimodal systems must serve all customers and stakeholders within the region and globally. Under the current grant, the new research projects and the ongoing research projects concentrate the program efforts on the categories of Transportation Systems Performance and Information Infrastructure to provide needed services to the New Jersey Department of Transportation, New York City Department of Transportation, New York Metropolitan Transportation Council, New York State Department of Transportation, and the New York State Energy and Research Development Authority and others, all while enhancing the center's theme.

Education and Workforce Development

The modern professional must combine the technical skills of engineering and planning with knowledge of economics, environmental science, management, finance, and law as well as negotiation skills, psychology and sociology. And, she/he must be computer literate, wired to the web, and knowledgeable about advances in information technology. UTRC's education and training efforts provide a multidisciplinary program of course work and experiential learning to train students and provide advanced training or retraining of practitioners to plan and manage regional transportation systems. UTRC must meet the need to educate the undergraduate and graduate student with a foundation of transportation fundamentals that allows for solving complex problems in a world much more dynamic than even a decade ago. Simultaneously, the demand for continuing education is growing – either because of professional license requirements or because the workplace demands it – and provides the opportunity to combine State of Practice education with tailored ways of delivering content.

Technology Transfer

UTRC's Technology Transfer Program goes beyond what might be considered "traditional" technology transfer activities. Its main objectives are (1) to increase the awareness and level of information concerning transportation issues facing Region 2; (2) to improve the knowledge base and approach to problem solving of the region's transportation workforce, from those operating the systems to those at the most senior level of managing the system; and by doing so, to improve the overall professional capability of the transportation workforce; (3) to stimulate discussion and debate concerning the integration of new technologies into our culture, our work and our transportation systems; (4) to provide the more traditional but extremely important job of disseminating research and project reports, studies, analysis and use of tools to the education, research and practicing community both nationally and internationally; and (5) to provide unbiased information and testimony to decision-makers concerning regional transportation issues consistent with the UTRC theme.

UTRC-RF Project No: 49997-31-24

Project Date: April 2014

Project Title: Energy Efficient and Environmental Friendly Cement Free Concrete (CFC) for Pavement and Bridge Deck Application

Project's Website:

<http://www.utrc2.org/research/projects/cement-free-concrete>

Principal Investigator:

Dr. Sulapha Peethamparan
Assistant Professor
236 Rowley Laboratories
Clarkson University
CU Box 5710
Potsdam, NY 13699-5710
Phone: 315-268-4435
Email: speetham@clarkson.edu

Co-Author: Robert Thomas

Performing Organization: Clarkson University

Sponsor:

University Transportation Research Center - Region 2, A Regional University Transportation Center sponsored by the U.S. Department of Transportation's Research and Innovative Technology Administration

To request a hard copy of our final reports, please send us an email at utrc@utrc2.org

Mailing Address:

University Transportation Research Center
The City College of New York
Marshak Hall, Suite 910
160 Convent Avenue
New York, NY 10031
Tel: 212-650-8051
Fax: 212-650-8374
Web: www.utrc2.org

Board of Directors

The UTRC Board of Directors consists of one or two members from each Consortium school (each school receives two votes regardless of the number of representatives on the board). The Center Director is an ex-officio member of the Board and The Center management team serves as staff to the Board.

City University of New York

Dr. Hongmian Gong - Geography
Dr. Neville A. Parker - Civil Engineering

Clarkson University

Dr. Kerop D. Janoyan - Civil Engineering

Columbia University

Dr. Raimondo Betti - Civil Engineering
Dr. Elliott Sclar - Urban and Regional Planning

Cornell University

Dr. Huaizhu (Oliver) Gao - Civil Engineering
Dr. Mark A. Turnquist - Civil Engineering

Hofstra University

Dr. Jean-Paul Rodrigue - Global Studies and Geography

Manhattan College

Dr. Anirban De - Civil & Environmental Engineering
Dominic Esposito - Research Administration

New Jersey Institute of Technology

Dr. Steven Chien - Civil Engineering
Dr. Joyoung Lee - Civil & Environmental Engineering

New York Institute of Technology

Dr. Nada Marie Anid - Engineering & Computing Sciences
Dr. Marta Panero - Engineering & Computing Sciences

New York University

Dr. Mitchell L. Moss - Urban Policy and Planning
Dr. Rae Zimmerman - Planning and Public Administration

Polytechnic Institute of NYU

Dr. John C. Falcocchio - Civil Engineering
Dr. Kaan Ozbay - Civil Engineering

Rensselaer Polytechnic Institute

Dr. José Holguín-Veras - Civil Engineering
Dr. William "Al" Wallace - Systems Engineering

Rochester Institute of Technology

Dr. J. Scott Hawker - Software Engineering
Dr. James Winebrake - Science, Technology, & Society/Public Policy

Rowan University

Dr. Yusuf Mehta - Civil Engineering
Dr. Beena Sukumaran - Civil Engineering

Rutgers University

Dr. Robert Noland - Planning and Public Policy

State University of New York

Michael M. Fancher - Nanoscience
Dr. Catherine T. Lawson - City & Regional Planning
Dr. Adel W. Sadek - Transportation Systems Engineering
Dr. Shmuel Yahalom - Economics

Stevens Institute of Technology

Dr. Sophia Hassiotis - Civil Engineering
Dr. Thomas H. Wakeman III - Civil Engineering

Syracuse University

Dr. Riyad S. Aboutaha - Civil Engineering
Dr. O. Sam Salem - Construction Engineering and Management

The College of New Jersey

Dr. Thomas M. Brennan Jr. - Civil Engineering

University of Puerto Rico - Mayagüez

Dr. Ismael Pagán-Trinidad - Civil Engineering
Dr. Didier M. Valdés-Díaz - Civil Engineering

UTRC Consortium Universities

The following universities/colleges are members of the UTRC consortium.

City University of New York (CUNY)
Clarkson University (Clarkson)
Columbia University (Columbia)
Cornell University (Cornell)
Hofstra University (Hofstra)
Manhattan College
New Jersey Institute of Technology (NJIT)
New York Institute of Technology (NYIT)
New York University (NYU)
Polytechnic Institute of NYU (Poly)
Rensselaer Polytechnic Institute (RPI)
Rochester Institute of Technology (RIT)
Rowan University (Rowan)
Rutgers University (Rutgers)*
State University of New York (SUNY)
Stevens Institute of Technology (Stevens)
Syracuse University (SU)
The College of New Jersey (TCNJ)
University of Puerto Rico - Mayagüez (UPRM)

** Member under SAFETEA-LU Legislation*

UTRC Key Staff

Dr. Camille Kamga: *Director, UTRC*
Assistant Professor of Civil Engineering, CCNY

Dr. Robert E. Paaswell: *Director Emeritus of UTRC and Distinguished Professor of Civil Engineering, The City College of New York*

Herbert Levinson: *UTRC Icon Mentor, Transportation Consultant and Professor Emeritus of Transportation*

Dr. Ellen Thorson: *Senior Research Fellow, University Transportation Research Center*

Penny Eickemeyer: *Associate Director for Research, UTRC*

Dr. Alison Conway: *Associate Director for New Initiatives and Assistant Professor of Civil Engineering*

Nadia Aslam: *Assistant Director for Technology Transfer*

Dr. Anil Yazici: *Post-doc/ Senior Researcher*

Nathalie Martinez: *Research Associate/Budget Analyst*

1. Report No.	2. Government Accession No.	3. Recipient's Catalog No.	
4. Title and Subtitle Energy Efficient and Environmentally Friendly Cement Free oncrete (CFC) for Pavement and Bridge Deck Application		5. Report Date 4/15/14	
		6. Performing Organization Code	
7. Author(s) Robert Thomas and Sulapha Peethamparan		8. Performing Organization Report No.	
9. Performing Organization Name and Address Clarkson University 236 Rowley Laboratories Clarkson University Potsdam, NY 13699-5710		10. Work Unit No.	
		11. Contract or Grant No. 49997-31-24	
12. Sponsoring Agency Name and Address University Transportation Research Center City College of New York 137th Street and Convent Avenue New York, NY 10031		13. Type of Report and Period Covered Final Report	
		14. Sponsoring Agency Code	
15. Supplementary Notes			
16. Abstract A comprehensive study was performed to develop energy efficient and environmentally friendly alkali-activated cement-free concrete mixtures for pavement and bridge deck applications using sodium silicate-activated fly ash and slag as the sole binders. The effects of water content, air entrainment, alkali concentration, and curing temperature and duration on the resulting compressive strength and workability were evaluated. From these data, four mixtures were selected that showed potential for application in transportation infrastructure. Three sodium silicate-activated slag mixtures and one sodium silicate-activated fly ash mixture were selected based on compressive strength, with a target range of 30-40 MPa, and with adequate workability. The selected mixtures were evaluated in detail to determine their applicability in terms of mechanical performance and long-term durability. To quantify mechanical performance, the compressive strength, tensile strength, elastic modulus, and Poisson's ratio were determined for the selected mixtures at both ambient and elevated temperature curing conditions. It was shown that the tensile strength of all mixtures was about 21% of the compressive strength, the elastic modulus was approximately 600 times the compressive strength, and the Poisson's ratio was most nearly 0.12. The current relationships for ordinary portland cement (OPC) concrete underestimate the tensile strength and overestimate the elastic modulus. The typical Poisson's ratio for OPC concrete is 0.18, about 50% higher than in alkali-activated concrete. The evaluated durability properties included the chloride penetrability, a measure of the potential for corrosion of steel reinforcement, alkali-silica reaction (ASR) potential, a measure of the susceptibility to deleterious expansion due to reactions between alkaline and siliceous materials within the concrete, and drying shrinkage, an indication of the susceptibility of concrete to shrinkage and cracking caused by removal of pore water. Results indicated high chloride penetrability for all mixtures, although this was likely an artifact of the test method. No trends were discernible with regard to ASR, since identical mixtures tested under two different methods gave conflicting results. Additionally, high-magnitude drying shrinkage was observed in the proposed mixtures when cured at ambient temperature. Drying shrinkage was drastically reduced in heat-cured specimens, but this was likely due to the loss of water during the heat curing process. Overall, the mixtures proposed cannot be put into practical use until the durability properties are investigated further. Additional methods of permeability measurement need to be employed, and further research into ASR must be performed. Additionally, it is necessary to investigate means of reducing the shrinkage of these mixtures prior to implementation.			
17. Key Words		18. Distribution Statement	
19. Security Classif (of this report) Unclassified	20. Security Classif. (of this page) Unclassified	21. No of Pages 73	22. Price

Disclaimer

The contents of this report reflect the views of the authors, who are responsible for the facts and the accuracy of the information presented herein. The contents do not necessarily reflect the official views or policies of the University Transportation Research Center (UTRC) or the Federal Highway Administration. This report does not constitute a standard, specification, or regulation. This document is disseminated under the sponsorship of the Department of Transportation, University Transportation Centers Program, in the interest of information exchange. The U.S. Government assumes no liability for the contents or use thereof.

Executive Summary

A comprehensive study was performed to develop energy efficient and environmentally friendly alkali-activated cement-free concrete mixtures for pavement and bridge deck applications using sodium silicate-activated fly ash and slag as the sole binders. The effects of water content, air entrainment, alkali concentration, and curing temperature and duration on the resulting compressive strength and workability were evaluated. From these data, four mixtures were selected that showed potential for application in transportation infrastructure. Three sodium silicate-activated slag mixtures and one sodium silicate-activated fly ash mixture were selected based on compressive strength, with a target range of 30-40 MPa, and with adequate workability. The selected mixtures were evaluated in detail to determine their applicability in terms of mechanical performance and long-term durability. To quantify mechanical performance, the compressive strength, tensile strength, elastic modulus, and Poisson's ratio were determined for the selected mixtures at both ambient and elevated temperature curing conditions. It was shown that the tensile strength of all mixtures was about 21% of the compressive strength, the elastic modulus was approximately 600 times the compressive strength, and the Poisson's ratio was most nearly 0.12. The current relationships for ordinary portland cement (OPC) concrete underestimate the tensile strength and overestimate the elastic modulus. The typical Poisson's ratio for OPC concrete is 0.18, about 50% higher than in alkali-activated concrete. The evaluated durability properties included the chloride penetrability, a measure of the potential for corrosion of steel reinforcement, alkali-silica reaction (ASR) potential, a measure of the susceptibility to deleterious expansion due to reactions between alkaline and siliceous materials within the concrete, and drying shrinkage, an indication of the susceptibility of concrete to shrinkage and cracking caused by removal of pore water. Results indicated high chloride penetrability for all mixtures, although this was likely an artifact of the test method. No trends were discernible with regard to ASR, since identical mixtures tested under two different methods gave conflicting results. Additionally, high-magnitude drying shrinkage was observed in the proposed mixtures when cured at ambient temperature. Drying shrinkage was drastically reduced in heat-cured specimens, but this was likely due to the loss of water during the heat curing process. Overall, the mixtures proposed cannot be put into practical use until the durability properties are investigated further. Additional methods of permeability measurement need to be employed, and further research into ASR must be performed. Additionally, it is necessary to investigate means of reducing the shrinkage of these mixtures prior to implementation.

Contents

1	Introduction.....	6
1.1	Mechanical and Engineering Properties of AAC	7
1.2	Chloride Ion Penetrability of Alkali-Activated Concrete.....	8
1.3	Alkali-Silica Reaction in Alkali-Activated Concrete	10
1.4	Drying Shrinkage of Alkali-Activated Concrete.....	11
1.5	Research Objectives	14
2	Materials and Methods.....	15
2.1	Materials	15
2.2	Mixture Proportion Method.....	17
2.3	Preparation Method	19
2.4	Curing Methods	19
2.5	Test Methods	20
2.6	Experimental Program.....	25
3	Results and Discussion.....	28
3.1	Phase One: Preliminary Experimentation.....	28
3.2	Phase Two: Mechanical and Engineering Properties	46
3.3	Phase Three: Durability Properties.....	53
4	Conclusions and Recommendations	61
5	Publication.....	65
A	Appendix I: Mixture Proportion Information.....	70

1 Introduction

Ordinary portland cement concrete is one of the most widely used materials for infrastructure, with production of Portland cement totaling 3.6 billion tons in 2011 [1]. The consumer cost of the concrete produced in the United States alone is nearly \$40 billion per year [1]. The Portland cement manufacturing process involves mining, grinding, and blending of raw minerals, clinkering in a rotary kiln at temperatures in excess of 1450°C, and milling, packaging, and transportation of the final product. These processes are all highly energy intensive. Manufacture of one ton of Portland cement requires 3.2-5.8 GJ energy, mainly from fossil fuels, and emits 0.95 tons of CO₂; this process is responsible for about 7% of global industrial CO₂ emissions [1-3]. The partial replacement of portland cement with fly ash and ground granulated blast furnace slag (GGBFS, or simply *slag*), a technique that has been employed since the mid-twentieth century, has served not only to reduce the environmental impact of concrete, but also to improve its workability, strength, and durability [4-7].

With increasing environmental regulations and energy costs, many industry professionals have sought means to replace portland cement entirely. Fly ash and slag are desirable replacement materials due to their ready availability and low cost. However, fly ash is pozzolanic [8, 9] and slag is only latently hydraulic [10, 11], meaning that it reacts slowly and incompletely in the presence of water. The addition of an alkaline element is necessary for strength development in both binder systems. In fly ash systems, the alkaline activator facilitates the dissolution of the amorphous material, allowing for the production of sodium aluminosilicate hydrate (N-A-S-H) gel [12-15]. In slag systems, alkali activation accelerates the hydraulic reaction by dissolving the impermeable glassy shell that forms around hydrating slag grains [16, 17].

Alkali activation of fly ash and slag is a rapidly advancing field, with numerous studies performed on the reaction kinetics, hydration products, and mechanical performance of alkali-activated concretes. Typical alkali activators include aqueous solutions of sodium carbonate, sodium phosphate, sodium hydroxide, and sodium silicate [16, 18-24]. The latter two are noticeably more common in the literature, but a few authors have suggested that liquid sodium silicates in particular are perhaps the most effective activators [12, 17, 20, 25]. Sodium silicates are solutions of sodium oxide (Na₂O), silica (SiO₂), and water and have sodium oxide concentrations as high as 7% (by mass of binder). The relative concentration of silica to sodium oxide is typically in the

range of 0.5 to 2.5; this ratio is the *silica modulus* (M_s). The ratio of activator solution to binding material, by mass, is commonly referred to as the solution/binder ratio (s/b).

Sodium silicate-activated slag (SS-Slag) concretes have been shown to develop strengths in the range of 30-60 MPa at both ambient temperature and with elevated temperature curing in the range of 50-70°C [16, 17, 26-28]. Similar strengths have been achieved with sodium silicate-activated fly ash concretes, although curing at temperatures as high as 85°C is typically necessary [12, 22, 29]. In addition to achieving relatively high strength, the durability of alkali-activated concretes has been shown to be improved over similar OPC concretes. Alkali-activated concretes show increased resistance to chloride ion penetration [26, 30, 31], increased resistance to acid attack [32-34], sulfate resistance similar to sulfate-resistant cements [35], and reduced potential for alkali-silica reaction [36-38]. Additionally, alkali activated fly ash and slag concretes have shown superior durability to OPC concrete under chemical exposure and freeze-thaw cycling [33, 39].

1.1 Mechanical and Engineering Properties of Alkali-Activated Concrete

For the purpose of concrete design, the modulus of elasticity of concrete is typically estimated using empirical relationships with the unit weight and compressive strength. For normal weight concrete, as specified by ACI-318, the modulus of elasticity is found by Equation **Error! Reference source not found.** after [43]. The equation can be simplified for normal weight concrete with unit weight of about 2320 kg/m³ (Equation **Error! Reference source not found.**).

$$E = 0.043 \times W_c \sqrt{f'_c} \quad (1)$$

$$E = 4700 \times \sqrt{f'_c} \quad (2)$$

where W_c is the unit weight in kg/m³ and f'_c and E are the compressive strength and static modulus of elasticity in MPa.

Carrasquilio [44] later showed that these relationships overestimate the modulus of elasticity of concretes with compressive strength above 41 MPa. In high strength concrete, coarse aggregate can become a strength and stiffness-limiting factor [45]. Additionally, microcracking in high strength concrete is less severe than in normal strength concrete at the same strain value [44]. ACI Committee 363 on high strength concrete adopted Equation **Error! Reference source not found.** for the modulus of elasticity of concrete with compressive strength above 41 MPa.

$$E = 3320 \times \sqrt{f'_c} + 6900 \quad (3)$$

The engineering properties of alkali-activated concretes have been studied by a few authors. Douglas, et al. [27] evaluated the compressive strength and elastic modulus of AAS concretes activated with sodium silicate and found that mixtures with compressive strength in the range of 40-50 MPA exhibited elastic moduli in the range of 25-30 GPa, much lower than would be expected for OPC concrete. Collins [17] showed similar results with elastic moduli in the range of 40 GPa for both heat-cured and ambient-cured sodium silicate-activated slag concrete. Finally, Swamy, et al. [46] found similar elastic moduli in the range of 30-40 GPa for even higher strength AAS concretes with compressive strengths in the range of 50-70 MPa. Fernandez-Jimenez, et al. [29] investigated the engineering properties of AAF concretes activated with both sodium hydroxide and sodium silicate solutions. Elastic moduli in the range of 10-20 GPa were observed for AAF concretes with compressive strength in the range of 30-40 MPa. These values are even lower than those seen by various researchers in AAS concretes. Very few studies have considered the tensile strength of alkali-activated concretes, and no conclusion regarding this were available in the literature.

1.2 Chloride Ion Penetrability of Alkali-Activated Concrete

The resistance of concrete to chloride ion penetration is an important property related to the long-term durability of reinforced concrete. Chloride-induced corrosion of steel reinforcement within structural concrete is one of the most costly infrastructure problems facing the transportation industry today. Concrete with low permeability, and therefore high resistance to chloride ion penetration, is required for the protection of transportation structures in cold climates where de-icing salts are prevalent.

A number of recent studies have investigated the chloride ion transport properties of AAC. Shi [47] evaluated various properties of AAS concretes activated with sodium carbonate, sodium silicate, and sodium hydroxide as compared to OPC concretes, including the chloride ion permeability. Rapid chloride penetrability testing (RCPT) indicated that AAS concretes were less permeable to chloride ions than OPC concrete, particularly when activated with sodium carbonate and sodium hydroxide. However, rapid temperature rise was observed during testing of sodium silicate-activated specimens, which was found to significantly increase the transport of chloride ions. It was additionally suggested that the RCPT result was more dependent on the chemistry of the pore solution than the pore structure of the concrete. The RCPT charge passed for all specimens in that study was high, in some cases in excess of 5000 coulombs, classifying the specimens as having high or very high chloride permeability.

These findings were echoed by a study by Al-Otaibi [48], who evaluated the chloride permeability of OPC, slag, and hybrid-binder concretes activated with sodium silicates. The study found that, in general, the chloride permeability of AAS concrete was lower than that of OPC concrete, but that the presence of highly concentrated alkalis gave potentially misleading results. It was additionally noted that the chloride permeability varied inversely with the silica modulus, or relative concentration of silica to sodium oxide in the activator solution. The RCPT charge passed for all alkali-activated slag concretes was below 2000 coulombs, classifying them as having either low or moderate chloride permeability.

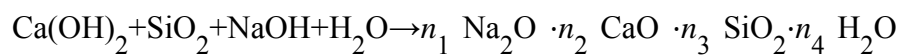
Bernal, et al. [49] evaluated the effect of binder content on several performance characteristics of alkali-activated slag concrete, including the chloride ion penetrability. For binder contents of 300, 400, and 500 kg/m³, it was shown that AAS concretes exhibited significantly lower chloride permeability than OPC concretes with the same binder content. The RCPT charge passed for these specimens was less than 1000 coulombs for AAC, and around 2000 coulombs for OPC concrete.

Ravikumar and Neithalath [31, 50] very recently performed an extensive study on the chloride transport properties of AAS concretes activated by liquid and powder sodium silicates. The study included permeability evaluation using RCPT, non-steady state migration (NSSM), microstructural and pore structure characterization, electrical impedance spectroscopy, and mercury intrusion porosimetry. The RCPT and NSSM estimates of chloride permeability were shown to be proportional to the silica modulus. Additionally, all measures of permeability indicated that powdered sodium silicate activators produce less permeable concrete. In general, AAS concretes performed better than OPC concretes with respect to permeability properties. A correlation was developed between the chloride permeability as determined by RCPT and the electrical resistivity of the bulk concrete.

Similar studies have been performed to investigate the chloride ion penetration resistance of alkali-activated fly ash concretes, although they are relatively few in number. Saraswathy and Song [51] evaluated the potential corrosion performance of steel embedded in blended fly ash (10-40% cement replacement with fly ash) concrete with and without activation by sodium carbonate. Techniques included RCPT and electrical resistivity measurement. It was observed that the chloride permeability was significantly reduced through additions of fly ash. The most significant permeability reduction occurred through the use of alkali activators in addition to partial cement replacement with fly ash.

1.3 Alkali-Silica Reaction in Alkali-Activated Concrete

Alkali-silica reaction in concrete describes the reaction between the alkaline pore fluid (a result of the sodium and potassium oxides in the cement) and siliceous aggregates. Although the reaction involved are highly complex and variable, they are assumed to behave similarly to the following, where NaOH represents the equivalent sodium or potassium oxide [37, 46]:



The reactions result in the formation of several crystalline alkali silicate species; in the presence of calcium hydroxide (CH), poorly crystalline C-S-H is also produced, adding further complexity to the system [6, 46]. The swelling of the ASR gels causes expansion pressure within the past matrix, causing 'map cracking' in the concrete [6, 46, 52]. ASR in concrete has been a topic of interest in the engineering literature since the early twentieth century, and is typically prevented by limiting the sodium and potassium oxides within the portland cement.

It would seem that AAC would be highly susceptible to ASR, but this is in fact a common misconception resulting from 'alkali-activated' terminology. The results of many experimental studies show that alkali-activated slag and fly ash concretes are less susceptible to ASR than OPC concretes [22, 33, 36-38]. However, Bakharev et. al. [41] reported that alkali-activated slag concretes showed significantly higher expansion due to ASR than OPC concrete, although this may be attributed to differences in the nature of the slag and of the reactive aggregate [22]. Small additions of supplementary cementitious materials in OPC concrete have also been shown to limit ASR expansion [53, 54]. It is generally accepted that the lack of portlandite (Ca(OH)_2) in the cement replacement material is a factor in limiting the ASR expansion in alkali-activated concrete [22, 53]. Despite the improvements in ASR resistance, it has been suggested that alkali-activated concretes are still susceptible to ASR expansion, but at a much slower rate than OPC systems [37].

1.4 Drying Shrinkage of Alkali-Activated Concrete

Drying shrinkage of concrete is a volumetric reduction as a result of the removal of physically adsorbed capillary water [55, 56]. The loss of capillary water produces tensile stresses within the concrete, causing shrinkage. In general, drying shrinkage of concrete varies inversely with relative humidity and aggregate content and directly with water/cement ratio [57-59]. Additional influencing factors include specimen geometry and mechanical properties of aggregate phases [56, 58]. A number of techniques have been proposed to limit or reduce the magnitude of drying shrinkage in concrete. Small additions of mineral admixtures like fly ash and silica fume have been shown to be effective at reducing the drying shrinkage of OPC concrete [60, 61]. Additionally, shrinkage reducing admixtures that reduce the surface tension of the pore fluid have resulted in reduced drying shrinkage [59, 62, 63]. It is typically recommended that drying shrinkage strain be limited to about 700 microstrain ($\mu\epsilon$) within a period of four months in order to prevent shrinkage cracking [64].

Significant work regarding the drying shrinkage of alkali-activated slag (AAS) concrete at Monash University in Australia. Collins and Sanjayan [17] compared the drying shrinkage of sodium silicate and sodium carbonate AAS concrete to that of OPC concrete. It was shown that while OPC concrete developed about 700 $\mu\epsilon$ drying shrinkage after 112 days, the sodium silicate-activated slag concrete developed over 1500 $\mu\epsilon$ drying shrinkage. Sodium carbonate-activated slag concrete developed about 1100 $\mu\epsilon$ at 112 days, although the shrinkage was nearly identical to OPC until about 56 days [17]. Despite the higher shrinkage in AAS concretes, it was noted that the moisture loss was larger for OPC concretes than for AAS. After a detailed study on the effect of pore size distribution on drying shrinkage, Collins and Sanjayan concluded that this effect was due to the prevalence of smaller pores within the AAS system. As the adsorbed pore water is removed, a meniscus forms around the pore radius and is responsible for the buildup of tensile stresses. Smaller pore radii, as in the AAS concrete, result in larger magnitude shrinkage strains [65]. Using restrained beam and ring cracking tests, the group observed that this high drying shrinkage drastically increased the tendency of AAS to crack. Cracks were observed in all AAS concretes after as little as 1-3 days of drying, while OPC concretes did not show appreciable cracks until about nine days. Later-age crack dimensions were about 0.97 mm for AAS at 175 days, while OPC showed crack widths of only 0.33 mm at the same age [66]. Despite this, large-scale AAS columns evaluated by the same researchers did not crack after 90 days of drying, while similar OPC concrete columns did show cracking. It was postulated that cracking of AAS was reduced at large scale due to the higher tensile strain capacity and lower elastic modulus of AAS concrete [67].

Collins and Sanjayan later investigated the effects of internal curing of alkali-activated slag concrete using soaked porous coarse aggregate. The results of this study indicated that the magnitude of drying shrinkage strain was reduced by 40% through additions of pre-soaked porous coarse aggregate. Shrinkage strain was reduced from nearly 1000 $\mu\epsilon$ at 56 days to about 400 $\mu\epsilon$, which was comparable to the shrinkage of OPC concrete at the same age [68]. Additionally, minor increases in compressive strength were noted due to internal curing. Further research investigated the effects of elevated temperature curing on the properties of alkali-activated slag concrete by comparing the properties of ambient temperature-cured concrete to those of concretes cured under two elevated temperature conditions: ramped temperature curing with a rest at 65°C and constant temperature curing at 70°C. It was shown that for both elevated temperature curing conditions, the drying shrinkage was approximately one-third that of ambient cured alkali-activated slag concrete. The drying shrinkage strain for both elevated temperature curing conditions was also less than that observed in OPC concretes [20]. The group also investigated the effect of several chemical admixtures on the properties of alkali-activated slag concretes. Several were found to reduce the drying shrinkage of the mixture tested. These included air entraining admixtures (AEA), glenium, and traditional shrinkage reducing admixtures (SRA). Lignosulphonate-based admixtures were found to result in a very slight drying shrinkage reduction, and naphthalene-based plasticizers were found to increase the shrinkage. The group concluded that air entrainers were the most suitable admixtures for use in alkali-activated concretes [41]. Palacios and Puertas similarly concluded that polypropylene glycol-based SRA reduced the drying shrinkage of sodium silicate-activated slag mortars, and that the SRA additionally retarded the activation of the binder [69, 70].

Relatively little information is available regarding the drying shrinkage of AAF concretes. Two studies were performed in which the drying shrinkage of AAF concretes were found to be significantly lower than those of OPC concretes. In some cases, AAF concretes were even shown to expand during drying cycles [29, 71]. Further research is necessary to expand the knowledge regarding the phenomenon of drying shrinkage within the context of AAC, particularly with respect to AAF systems.

1.5 Research Objectives

Despite the many advantages of alkali-activated concrete, many questions have been raised with regard to their appropriateness and practicality as a real-world construction material. These problems include poor workability and rapid slump loss, especially with high solution concentration [17, 40, 41], and slow strength development, particularly in fly ash systems [22]. The former is problematic for placement and consolidation, while the latter hinders rapid construction. Additionally, a few studies have suggested that alkali-activated concretes may be highly susceptible to shrinkage and have a high occurrence of microcracking [17, 23, 40, 42]. All of these drawbacks limit the potential for application of alkali-activated cement-free concrete in construction. The purpose of this study is to investigate and develop practical alkali-activated concrete mixtures using sodium silicate -activated class C fly ash (SS-F) and slag (SS-S). The strength development under various curing conditions will also be investigated. Mechanical properties including compressive and tensile strength, elastic modulus, and Poisson ratio will be determined, and strength estimates will be found using non-destructive methods. Finally, various durability properties will be measured, including porosity, shrinkage, alkali-silica reaction (ASR) potential, and chloride permeability.

The following objectives are identified and outlined for this study:

1. Evaluate the effect of several parameters including activator solution concentration, curing condition, water content, and admixture dosage on the compressive strength and workability of SS-F and SS-S concrete mixtures.
2. Identify several optimal mixtures that are practical for construction.
3. Evaluate the mechanical and engineering properties of the selected mixtures, including compressive strength, tensile strength, elastic modulus, and Poisson's ratio.
4. Evaluate the durability properties of the selected mixtures including permeability, drying shrinkage, and alkali-silica reaction potential.
5. Disseminate findings in the context of bridge deck and transportation infrastructure applications and compare the performance of alkali-activated concretes to those of OPC concretes typically used for these applications.

2 Materials and Methods

2.1 Materials

2.1.1 Binders

The binder materials used in this study were ground granulated blast furnace slag (GGBFS, or *slag*) and fly ash. The slag was a grade 100, ASTM C 989-compliant blast furnace slag and the fly ash was a high-calcium (Class C) coal fly ash. Both binders were from reputable commercial suppliers; slag was provided by Holcim, USA (Chicago, IL) and fly ash was provided by Lafarge North America (Pleasant Prairie, WI).¹ The chemical oxide composition of the binder materials are listed in Table 1.

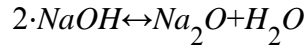
Table 1: Chemical Oxide Composition of Binder Materials

Composition % by mass	Slag	Fly Ash
SiO ₂	36.0	37.7
Al ₂ O ₃	10.5	20.0
CaO	39.8	23.4
MgO	7.9	4.3
Na ₂ O	0.3	1.7
SO ₃	2.1	2.4
K ₂ O	0.2	0.6
Fe ₂ O ₃	0.7	5.6

¹ Supplier information is included for informative purposes only. Such information does not imply endorsement by the authors or by Clarkson University, nor does such identification guarantee that the materials used here are the best for the presented applications.

2.1.2 Activators

The activator used throughout the study was an alkaline sodium silicate solution containing sodium oxide (Na_2O), silica (SiO_2), and pure deionized water. A reagent-grade manufactured solution of 10.6% Na_2O and 26.5% SiO_2 was used as a base solution. The relative concentration of SiO_2 and Na_2O was adjusted by additions of pure nano-silica, 98% pure reagent grade sodium hydroxide, and de-ionized water. Sodium hydroxide was assumed to dissociate in the following manner; for practical purposes, this means that it is assumed that NaOH dissociates into 75.9% Na_2O and 24.1% H_2O by mass.



The concentration of Na_2O and SiO_2 in sodium silicate solutions is described by two parameters: sodium oxide concentration, % Na_2O (by mass of binding agent) and silica modulus, M_s , the mass of silica relative to sodium oxide (Eq. 4).

$$M_s = \frac{\text{SiO}_2}{\text{Na}_2\text{O}} \quad (4)$$

2.1.3 Aggregates

The coarse aggregate was a well-graded, semi-angular, natural gravel composed predominately of quartz. The nominal maximum particle size was 9.5 mm, the bulk density was 1560 kg/m^3 , and the specific gravity was approximately 1.64. The fine aggregate was a natural sand with a specific gravity of 1.70 and a fineness modulus of 2.54. The gradation curves are presented in Fig. 1.

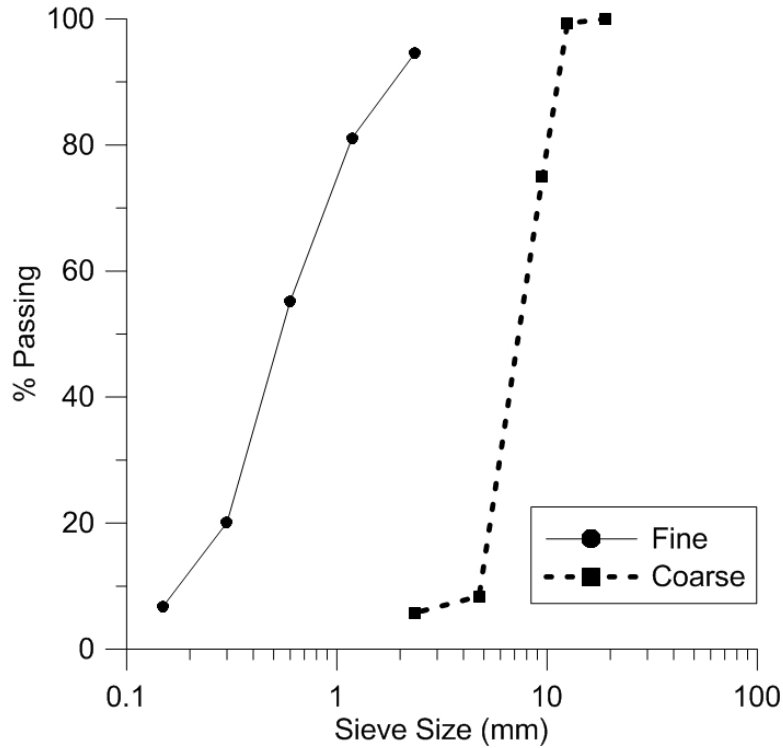


Figure 1: Fine and coarse aggregate gradation curves, in log scale.

2.2 Mixture Proportion Method

The mixture proportions used throughout this study were developed in accordance with the absolute volume method prescribed by the Portland Cement Association (PCA) Guide for the Design and Control of Concrete Mixtures [72], with appropriate modifications. The mixture proportioning procedure was as follows:

1. **Determine solution content.** In the case of OPC concrete, the water content is specified based on the required workability (slump). However, in the case of AAC, an activator solution made up of water and dissolved alkalis is used in place of pure water. Thus, the solution content of the mixture is typically specified. The free water content—that is the quantity of pure water present in the solution—can be specified, but since the concentration of alkalis affects the free water content of the solution, this is typically calculated for informative rather than prescriptive purposes. Since the solution is not entirely water, the maximum recommended w/c of 0.45 was not considered for AAC. The desired slump for all mixtures was 75-100 mm, which is a typical range for mass concrete, slabs, bridge decks,

columns, and beams. A solution content of 228 kg/m^3 was selected for all mixtures, which was lower than the PCA recommended value, but produced reasonably workable mixtures that were not prone to segregation.

2. **Determine binder content.** In the case of OPC concrete, the cement content is determined based on the specified water-cement ratio (w/c), which is determined from PCA based on the desired compressive strength. In the case of AAC, however, the binder content was determined by the solution-binder ratio (s/b), which is simply the mass ratio of activator solution to binder material (fly ash or slag). The free water-binder ratio (fw/b) was determined based on the free water content as previously described.
3. **Determine coarse aggregate content.** As with OPC concrete, the coarse aggregate content was determined from the bulk volume based on the nominal maximum particle size of the coarse aggregate and the fineness modulus of the fine aggregate. Based on the characteristics of the aggregates used in this study, a bulk volume of 0.50 was used for all mixtures. The bulk density of the coarse aggregate was 1560 kg/m^3 , and so a coarse aggregate content of 780 kg/m^3 was used for all mixtures.
4. **Determine fine aggregate content.** As with OPC concrete, the fine aggregate content was determined based on the absolute volume method. The cumulative volume of coarse aggregate, binder, and solution were determined, and the remaining volume required for one cubic meter was the fine aggregate volume. The mass was computed based on the specific gravity of the fine aggregate.
5. **Determine admixture content.** Many studies have suggested the use of air entraining agents (AEA) to improve the workability of AAC, and so this technique was employed throughout the study. The correct dosage of admixture was determined based on the results of an experiment described later in this report. AEA was dosed relative to the mass of the binder.
6. **Determine activator solution contents.** As previously stated, the activator solution was a liquid sodium silicate solution composed of pure water, silica (SiO_2), and sodium oxide (Na_2O). The sodium oxide content was determined based on the specified concentration ($\%\text{Na}_2\text{O}$) relative to the mass of the binder, and the silica content was determined based on the

specified relative mass of silica to sodium oxide (M_s , or silica modulus). The remainder of the required solution mass was added as pure deionized water.

2.3 Preparation Method

Mixing and casting was performed in accordance with a strict protocol developed empirically based on the procedures that provided the highest quality specimens. Aggregates were prepared and stored in sealed containers at saturated surface dry condition several days in advance. Activator solutions were prepared at least 24 hours prior to casting to allow for dissolution and heat dissipation. This was especially important for solutions that required additions of NaOH, which sometimes created temperatures as high as 60°C. Aggregates and binders were batched first and mixed by hand to promote homogeneity in the mixture. This was followed by the addition of the activator solution, which was allowed to permeate the dry ingredients for 30 seconds and was then mixed for 30 seconds. Air-entraining agent, if specified, was added at this point. The sides of the container were scraped, and mixing continued for 90 seconds. Specimens were filled in two or three lifts and vibrated to promote consolidation. Additional hand tamping with a steel tamping rod was required for the harshest mixtures. All specimens were well sealed to avoid moisture loss during curing.

2.4 Curing Methods

Specimens were cured at both elevated and ambient temperatures throughout this study. All specimens were kept in sealed containers within the curing environment. Elevated temperature curing was completed in a high precision mechanical convection oven with temperature variation within 1°C. After the specified curing duration, specimens cured at elevated temperature were removed from the oven and placed in an insulated chamber. This was done to allow the specimens to cool to ambient temperature slowly, avoiding any damage that might be caused by rapid temperature fluctuation. Specimens cured at ambient temperature were placed in a chamber with humidity in excess fo 95%RH and temperature of 22±2°C.

2.5 Test Methods

2.5.1 Compressive Strength Evaluation

Compressive strength of concrete mixtures was evaluated in accordance with the specifications of ASTM C39 using 100x50 and 300x150 mm cylindrical specimens. Compressive strength testing was performed using a 1.1 MN capacity hydraulic test frame at a loading rate of approximately 0.25 MPa/s. Specimen faces were ground flat and parallel and neoprene rubber capping pads were provided to reduce any stress concentrations due to surface irregularities.

2.5.2 Tensile Strength Evaluation

Tensile strength evaluation was performed using the splitting tension method in accordance with the specifications of ASTM C496. 150x300 mm cylindrical concrete specimens outfitted with bearing blocks and plywood bearing strips were loaded in a 1.1 MN capacity hydraulic test frame at a rate of approximately 1 MPa until splitting failure occurred. The tensile strength was estimated by Eq. 5 where f_{sp} is the splitting tensile strength, P is the measured splitting force, and l and d are the length and diameter of the specimen.

$$f_{sp} = \frac{2P}{\pi ld} \quad (5)$$

2.5.3 Engineering Property Evaluation

The engineering properties (*i.e.*, *elastic modulus and Poisson's ratio*) of concrete mixtures were evaluated in accordance with the specifications of ASTM C469. 150 x 300 mm cylindrical concrete specimens were tested using a 500-kN servo-hydraulic load frame at a very slow strain rate of 6.67×10^{-4} /min (0.1 mm/min) to produce quasi-static conditions. Axial strain was measured using an electric extensometer with a gage length of 30 mm mounted at mid-height on the specimen, as well as two linear potentiometers mounted vertically in diametrically opposed positions on the test setup. Lateral strain was measured using a chain-type radial extensometer mounted at mid-height on the specimen. The test setup is shown in Fig. 2.

Specimens were preloaded to 40% of the ultimate compressive strength twice to allow for gage seating. Specimens were then loaded to 40% of the ultimate compressive strength and the strain measurements were recorded at a rate of about 1 Hz. The extensometers were then removed to prevent gage damage, and the specimen was loaded to failure with measurements taken using only the linear potentiometers.

The elastic modulus was calculated as the chord modulus, or a linear interpolation from the stress corresponding to 50 microstrain to the strain corresponding to 40% of the ultimate compressive strength (Eq. **Error! Reference source not found.**). Poisson's ratio was calculated as the ratio of the change in lateral strain to the change in axial strain over the same period (Eq. **Error! Reference source not found.**).

$$E = (S_2 - S_1)/(\epsilon_2 - \epsilon_1) \quad (6)$$

where:

E = chord modulus of elasticity

S_1 = stress corresponding to axial strain (ϵ_1) of 5×10^{-5}

S_2 = stress corresponding to 40% compressive strength

ϵ_2 = axial strain corresponding to 40% compressive strength

$$\mu = (\epsilon_{t2} - \epsilon_{t1})/(\epsilon_2 - \epsilon_1) \quad (7)$$

where:

μ = Poisson's ratio

$\epsilon_1 = 5 \times 10^{-5}$

ϵ_{t1} = transverse strain corresponding to ϵ_1

ϵ_2 = axial strain corresponding to 40% compressive strength

ϵ_{t2} = transverse strain corresponding to 40% compressive strength



Figure 2: Engineering property test setup. Axial strain was measured using the axial extensometer and linear potentiometers as shown. Lateral strain was measured using the radial extensometer as shown.

2.5.4 Drying Shrinkage Evaluation

Drying shrinkage is a volumetric reduction of concrete caused by the removal of capillary water. Excessive drying shrinkage can cause cracking or warping due to the development of internal tensile stresses. In this study, drying shrinkage was determined by the linear shrinkage of slender concrete prisms using the length comparator method in accordance with the specification of ASTM C490.

Slender concrete bars were cast having a 50 mm square cross-section and an effective gage length of 254 mm. Stainless steel gage studs were embedded into the fresh concrete and specimens were cured for 72 hours in a sealed environment at the specified curing temperature. Specimens cured at elevated temperatures were removed from the elevated temperature environment after 48 hours and allowed to cool to ambient temperature for 24 hours. Length readings were taken as the relative length of the specimen compared to an invar reference bar. Length measurements were taken periodically until there was no change during successive weeks. Shrinkage strain was calculated as the ratio of the length change and the initial gage length.

2.5.5 Chloride Ion Penetrability

The permeability of concrete is an important property related to the long-term durability of steel-reinforced concrete. Highly permeable concrete is susceptible to the ingress of chloride ions which cause corrosion of embedded steel reinforcement. This is of particular importance for transportation infrastructure in cold climates that require the use of de-icing salts.

In this study, the rapid chloride penetrability test (RCPT) was used to evaluate the permeability of concrete. This test provides an electrical indication of chloride ion penetrability, which is directly related to the permeability. The test was performed in accordance with the standards of ASTM C1202.

The RCPT setup is pictured in Fig. 3. One face of an epoxy-coated and vacuum-saturated concrete disk is exposed to a 3% solution of sodium chloride and the other is exposed to a 0.3N solution of sodium hydroxide. A 60V electrical potential is applied across the two faces forming an electrochemical cell. The total current that passes through the electrochemical cell corresponds to the movement of chloride ions through the concrete specimen. The chloride penetration is reported as the total current, in coulombs, that is measured over the course of six hours. Chloride penetrability is classified according to the categories listed below (ASTM C1202).

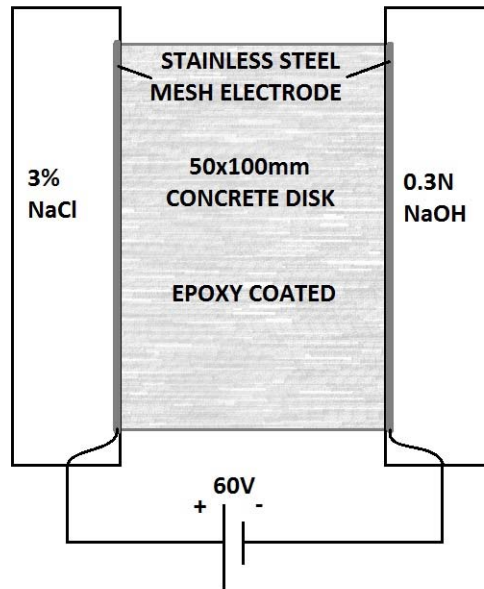


Figure 3: Rapid chloride penetrability test (RCPT) setup. Electrical resistivity is correlated to chloride ion penetration resistance.

2.5.6 Alkali-Silica Reaction Potential

Alkali-silica reaction potential was evaluated by both slow and accelerated methods. The slow method, performed in accordance with the specifications of ASTM C227, involved the storage of 25 x 25 x 254 mm mortar bars in a very high-humidity chamber for 14 days at a temperature of 38° C. Length measurements were taken using the length comparator method in accordance with the specifications of ASTM C157. Length was measured to the nearest 0.025 mm relative to a 254 mm invar reference bar. Measurements were taken before and after storage, and expansion was reported as the ratio of length change to initial length.

The accelerated method, performed in accordance with the specification of ASTM C1567, involved the storage of 25 x 25 x 254 mm mortar bars immersed in water at 80°C for one day and in 1M sodium hydroxide (NaOH) at 80°C for 14 days. Measurements were taken prior to immersion in NaOH, and three times during the 14-day immersion period in the same manner as previously described. Expansion was again reported as the ratio of length change to initial length.

2.6 Experimental Program

The experimental work outlined within this study was performed in three phases:

1. Determination of significant mixture parameters for AAC and their effect on performance, and selection of several appropriate mixtures for further investigation.
2. Evaluation of engineering and mechanical properties of selected AAC mixtures.
3. Evaluation of durability properties of selected AAC mixtures.

2.6.1 Phase One: Preliminary Experimentation

The first phase of the study was carried out to determine the effect of a variety of mixture parameters on the performance of AAC and to identify several mixtures that are appropriate for application in transportation structures. Parameters studied were concentration of sodium oxide, silica modulus, dosage of air entraining agent, solution-binder ratio, and curing temperature/duration. 100 x 50 mm cylindrical concrete specimens were cast from dozens of unique mixture proportions. These mixtures were evaluated qualitatively for workability and ease of casting, and were evaluated quantitatively for compressive strength. Sodium oxide concentrations were varied between 0 and 7% by mass fo binder, silica moduli were between 0.75 and 3.5, solution-binder ratios were between 0.40 and 0.50, and air entrainer dosages were between 0 and 0.5% by mass of binder. Curing conditions included ambient temperature curing for 28 days and elevated temperature curing at 50 and 75°C for 48 or 72 hours.

2.6.1.1 Evaluation of the Effect of AEA Dosage

Air entrainment was used to improve the workability of the mixtures used in this study. It was expected that the workability of mixtures would increase with the AEA dosage, however excessive dosage would result in a reduction in strength over the non air-entrained concrete. In order to determine the optimal dosage, 12 batches of SS-Slag concrete with three mixture proportions and four admixture dosages were cast. The sodium oxide concentration was 2.5% by mass of slag, the silica modulus was 2.5, and the solution/binder ratio was 0.4, 0.45, or 0.5. These solution/binder ratios were selected because they represent a spectrum of workability. AEA dosage was in the range of 0 to 0.5% by mass of slag. Specimens were cured at 50°C for 48 hours.

2.6.1.2 Evaluation of the Effect of Elevated Temperature Curing

An understanding of the effect of curing temperature and duration on the compressive strength of alkali-activated concrete was necessary in order to determine an appropriate accelerated curing method. It was desired to rapidly replicate the 28-day ambient temperature-cured strength using elevated temperature curing. Ten batches of SS-FAC concrete were cast and cured at ambient temperature (23±2°C) for 28 days or at elevated temperature (50 or 75°C) for 48 or 72 hours. The sodium oxide concentration was 2.5% by mass of fly ash, the silica modulus was 2.5, and the solution/binder ratio was 0.45.

2.6.1.3 Evaluation of the Effect of Alkali Concentration

Since it has been suggested that the alkali concentration (sodium oxide concentration and silica modulus) have a more significant effect on the properties of alkali-activated concrete than the water content or solution/binder ratio, this study focused on the effects of sodium oxide concentration (%Na₂O by mass of binder) and silica modulus (M_s , relative concentration of SiO₂/Na₂O). It has been suggested that the optimum silica modulus for alkali-activated slag is around 0.75 [20] and the authors have identified a practical limit of about 2.5. Therefore, the silica moduli selected for these experiments were 0, 0.5, 0.75, 1.0, 1.5, and 2.5. Sodium oxide concentration were between 0.5 and 6% by mass of slag. Similarly, it has been suggested that 1.5 is the optimum silica modulus of alkali-activated fly ash. Therefore, silica moduli of 0, 0.5, 1.0, 1.5, and 2.0 were tested with sodium oxide concentration between 1 and 8% by mass fo fly ash. All mixtures included 0.1% AEA by mass of binder. Most were cured at 50°C for 48 hours, but a few fly ash specimens were cured at 75°C for 48 hours.

2.6.1.4 Evaluation of Ambient Temperature Compressive Strength Development

Once the effect of solution concentration on compressive strength had been determined, it was important to both verify that similar strengths could be achieved with 28-day ambient temperature curing, and to characterize the early-age compressive strength development at ambient temperature. Three mixtures that resulted in relatively high strengths were selected based on the previous experimental results, and were cured at ambient temperature. Compressive strength was measured as soon as the specimens could be demolded, as well as at 7, 14, and 28 days. The 28-day compressive strength was compared to the previously recorded compressive strength for each mixture.

2.6.2 Phase Two: Mechanical and Engineering Properties

Once four mixtures had been identified as being potentially appropriate for application in transportation, the mechanical and engineering properties of these mixtures were evaluated. For each selected mixture, four sets of three 150 x 75 mm cylindrical specimens were cast. Two sets were cured at elevated temperature (50°C for 48 hours) and two were cured at ambient temperature (22°C for 28 days). From each set, one specimen was tested for compressive strength, one for splitting tensile strength, and one for elastic modulus and Poisson's ratio.

2.6.3 Phase Three: Durability Properties

Each of the four selected mixtures were also evaluated for durability properties. These included alkali-silica reaction potential, chloride ion penetrability, and drying shrinkage.

3 Results and Discussion

3.1 Phase One: Preliminary Experimentation

3.1.1 Effect of Preparation Method on Compressive Strength of AAC

It was determined during preliminary experimentation that the AAC compressive strength specimens were very sensitive to microcracking, particularly when test surfaces were prepared by cutting with a wet diamond saw. Cracking of specimens caused by this preparation method can be seen in Fig. 4. This is a possible indication of increased brittleness. Results from specimens prepared in this manner were discarded. All further compressive strength specimens were prepared by lightly polishing with a silicon carbide belt and capping with neoprene rubber pads (ASTM C1231).

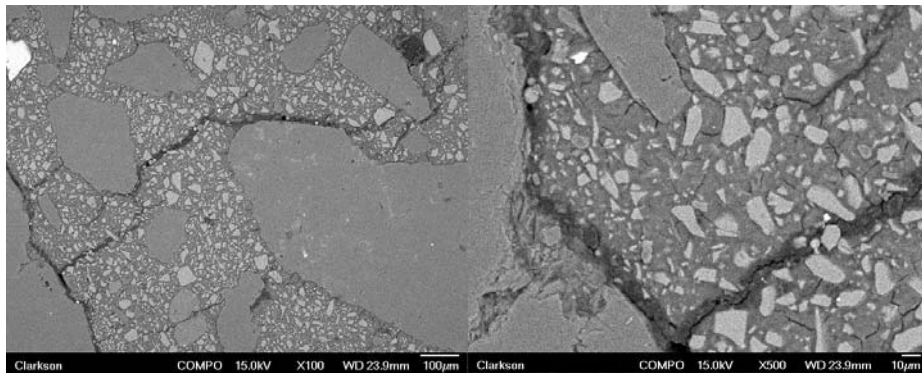


Figure 4: SEM images of NSH-Slag concrete show cracking caused by diamond saw cutting.

3.1.2 Effect of Solution-Binder Ratio on Compressive Strength of AAC

In order to determine the effect of solution-binder ratio on the compressive strength of AAC, 99 unique mixtures of AAS concrete were cast with various solution-binder ratios, silica moduli, and sodium oxide concentrations. 100x50 mm cylindrical specimens were cast in batches of 4, cured at 50°C for 48 hours, and cooled to room temperature. The complete mixture proportions are listed in Table 7 in the appendices.

Figure 5 and Table 2 show the average compressive strength of AAS concretes with 2.5% Na₂O, solution/binder ratio between 0.4 and 0.55, and silica modulus between 1.5 and 3.5. In general, compressive strength increases with increased silica modulus and decreases with increased solution/binder ratio. As expected, a few general trends emerged. Primarily, it was noted that increased silica modulus between 1.5 and 2.5 resulted in increased compressive strength. However, when silica modulus increased above 2.5, the strength was reduced. At a silica modulus of 3.5, the activator solution was very viscous due to the additions of solid silica. It was also noted that the solution-binder ratio had a relatively small effect on the compressive strength.

Several additional mixtures were cast having silica modulus of 3.5 and sodium oxide concentrations of 2.5 and 3.37% by mass of binder in order to determine the combined effect of solution-binder ratio and sodium oxide concentration on the compressive strength. Solution-binder ratios of 0.40, 0.45, and 0.50 were evaluated. Figure 6 shows the average compressive strength results. As expected, increased sodium oxide concentration resulted in increased strength. However, most mixtures were poorly workable and difficult to cast. The best performing mixtures with respect to strength were those with the lowest solution-binder ratios. In the case of high sodium and high silica, though, the mixture with solution-binder ratio of 0.50 exhibited higher strength than the mixture with 0.45 solution-binder ratio. This was likely due to improved consolidation, although inspection of failed specimen revealed significant segregation in specimens with 0.50 solution-binder ratio. This indicates that the early workability is sensitive to the water content, since high solution-binder ratio resulted in segregation which is an indication of a very loose mixture. Additionally, the rate of slump loss seems to be sensitive to the activator concentration, since mixtures set very quickly. High water content resulted in segregation prior to early setting, while low water content resulted in poor consolidation prior to the same early setting. Based on the results seen here, the optimum water content corresponds to a solution-binder ratio between 0.4 and 0.45. A silica modulus of 3.5 resulted in impractically low setting times, and so a maximum of 2.5 was established.

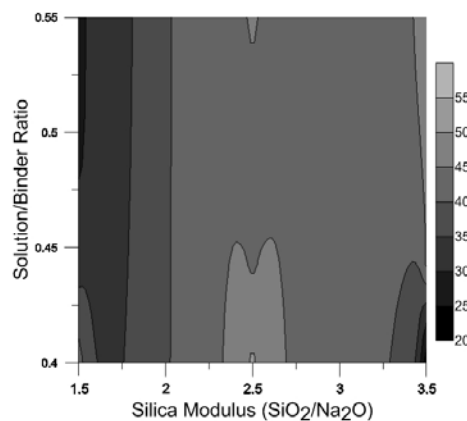


Figure 5: Compressive strength of AAS concrete with varying silica modulus (M_s) and solution/binder ratio (s/b).

Table 2: Average compressive strength (MPa) of AAS concrete

		Silica Modulus		
		1.5	2.5	3.5
Solution/ Binder	0.40	42.3	50.9	22.2
	0.45	32.1	44.0	46.4
	0.50	28.2	40.7	46.3
	0.55	29.4	46.1	48.2

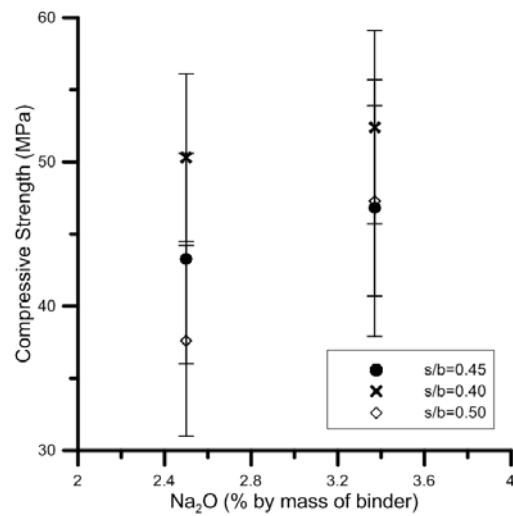


Figure 6: Compressive strength of AAS concrete with 2.5% and 3.37% Na₂O and M_s=2.5.

3.1.3 Effect of Air Entraining Agent (AEA) on Compressive Strength of AAC

Due to the poor workability and difficulty in casting many of the mixtures tested, it was determined that chemical admixtures were necessary to provide mixtures that were adequately workable to be cast without significant voids. A few researchers suggest that air entraining agents (AEA) are the most practical means of adjusting the workability of AAC, and so the effect of an AEA provided by Sika was evaluated. AAS concrete with silica modulus of 2.5 and 2.5% sodium oxide by mass of binder was selected for evaluation. Three solution-binder ratios were evaluated: 0.40, which resulted in very poorly workable concrete, 0.45, and 0.50, which were both very workable. These mixtures were chosen in order to evaluate the effects of AEA dosage on both harsh and loose mixtures. AEA dosages of 0, 0.1, 0.3, and 0.5% by mass of binder were evaluated, and it was assumed that any strength increases over the neat (non-air-entrained) strength were due to improved consolidation. The complete mixture proportions are listed in Table 8 in the appendices.

The neat compressive strengths were 42.3, 43.2, and 46.5 MPa, respectively for solution/binder ratios of 0.4, 0.45, and 0.5. The relative compressive strengths of specimens with AEA dosage ranging from 0-0.5% by mass of slag are plotted in Figure 7. The figure shows the air-entrained compressive strength relative to the neat compressive strength. A value of 1.0 indicates that the air-entrained strength is equal to the neat compressive strength. Almost all mixtures showed increased compressive strength with air entrainment, which was attributed to enhanced compaction. Some mixtures-namely those with $s/b=0.5$ and AEA dosage above 0.1%-had reduced strength, which was attributed to excessive segregation, as well as the strength reduction effect of the air entrainment [73, 74]. The most significant strength improvements were seen with solution/binder ratio of 0.4 due to the fact that the poor initial workability led to the formation of large voids. Even a small dosage of 0.1% AEA was adequate to correct this. Dosages above 0.1% did not improve strength as significantly, most likely due to the strength reduction effect of the entrained air. No significant differences in compressive strength were detected for any AEA dosage at higher solution/binder ratios, based on hypothesis testing at a 95% confidence level. The optimum dosage of AEA-15 was identified as 0.1% based on these results. This value was chosen because it resulted in markedly improved workability in all mixtures, significant strength improvements in harsh mixtures, and no significant strength differences in other mixtures.

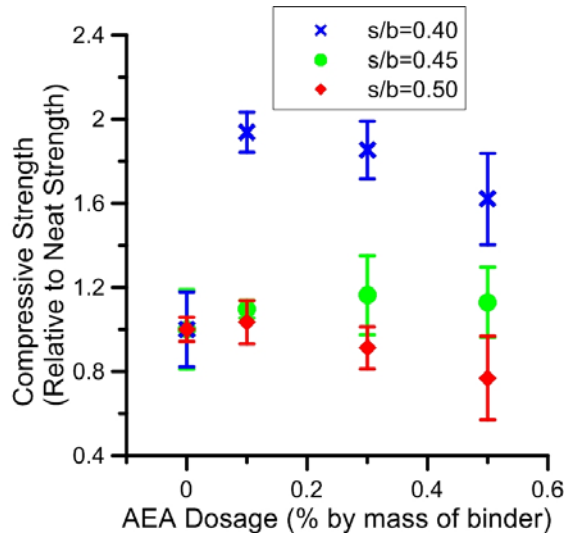


Figure 7: Ratio of compressive strengths of air-entrained and neat SS-Slag concrete (50°C, 48 hr).

3.1.4 Effect of Curing Temperature and Duration on Compressive Strength of AAC

In order to determine the effect of curing temperature and duration of the resulting compressive strength of AAC, several identical batches of AAF concrete with silica modulus of 2.5, sodium oxide concentration of 2.5% by mass of binder, and solution-binder ratio of 0.45 were cast and cured at temperatures of 50 and 75°C for durations of 48 and 72 hours. Additional identical specimens were cast at ambient temperature (22°C) for 28 days. The complete mixture proportion is listed in Table 9 in the appendices. The 28-day ambient-cured compressive strength was approximately 14 MPa. The relative compressive strengths of the elevated temperature-cured specimens are plotted in Fig. 8. The plot shows the ratio of the elevated temperature cured strength to the ambient compressive strength, where a value of 1.0 indicates identical strength.

Curing at 50°C for 48 or 72 hours resulted in approximately the same compressive strength as 28-day ambient curing. Curing at 75°C results in strength increases of 80% and 140% over 28-day ambient strength for 48 and 72 hours, respectively. Based on these results, it was determined that curing at 50°C for 48 hours would most closely replicate the 28-day strength when cured at ambient temperature. Additionally, these results indicate that the temperature may be more significant than the curing duration in the determination of compressive strength.

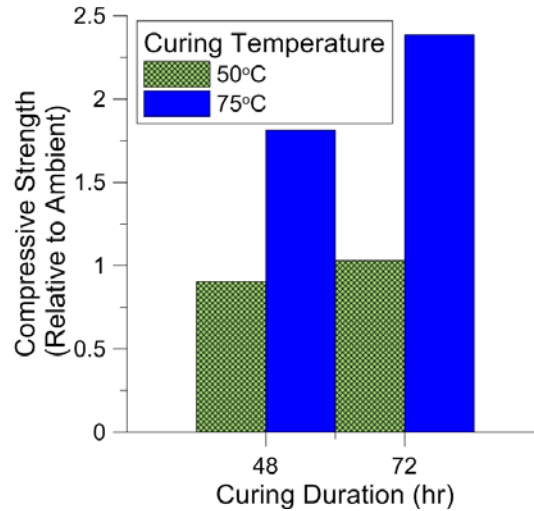


Figure 8: Ratio of compressive strengths of heat-cured and 28-day ambient temperature-cured AAF concrete.

In addition to the compressive strength development at elevated temperature, the development of compressive strength at ambient temperature was also evaluated for both AAF and AAS concretes. For this experiment, AAF concrete had a silica modulus of 1.0 and sodium oxide concentration of 6.0% by mass of binder and AAS concrete had a silica modulus of 0.75 and 5.0% sodium oxide by mass of binder. The solution-binder ratio was 0.40 for both mixtures and both included 0.1% AEA dosage. The complete mixture proportions are listed in Tables 10 and 11 in the appendices.

The compressive strength was measured as soon as specimens could be demolded without suffering mechanical damage. This corresponded to an age of about three days, and a compressive strength of about 10 MPa. The compressive strength at 3, 7, 14, and 28 days is plotted in Figure 9 for both mixtures. Both mixtures showed steady strength gain over the first 28 days, and both reached approximately the same strength developed after elevated temperature curing. This was the expected result, as indicated by previous discussions on elevated temperature curing. These results indicate that AAF concrete may not be appropriate for normal construction scenarios, since heat-curing is necessary for the development of adequate compressive strength. Despite this, applications for SS-FAC concrete may exist in the precast industry. On the other hand, AAS concretes appear to be more appropriate for construction in terms of ambient temperature strength development.

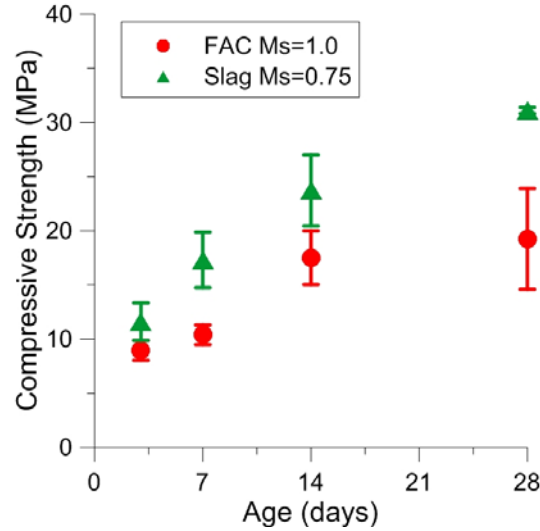


Figure 9: Compressive strength of fly ash and slag concrete at 3, 7, 14, and 28 days.

3.1.5 Effect of Alkali Concentration on Compressive Strength of AAC

3.1.5.1 Sodium Silicate-Activated Slag

The compressive strength of AAS concrete with solution/binder ratio of 0.40, 0.1% AEA dosage by mass of slag, and cured at 50°C for 48 hours is plotted in Figures 10. The complete mixture proportions of all mixtures are listed in Table 12 in the appendices. This contour plot is an estimate of the compressive strength relationships prepared using a power function-based smoothing algorithm; it does not serve as a model, but rather as a means of identifying general trends and areas of best performance. It can be seen that strength generally increases with both silica modulus and sodium oxide concentration, but that the compressive strength did not reach an acceptable level with lower silica moduli. It is expected that this could be corrected by increasing sodium oxide concentration. However, the production of sodium oxides is very energy-intensive relative to the commercial processing of common sources of silica, and so limiting the sodium oxide concentration is desirable.

The compressive strength of AAS concrete with silica moduli of 0.75, 1.5, and 2.5 is plotted in Figure 11. Strength in the 30-40 MPa range were achieved at all three silica moduli, but increased sodium oxide concentration was necessary with lower silica modulus. At a silica modulus of 2.5, 30 MPa strength was attained at only 1.5% Na₂O concentration. SS-Slag concrete with silica modulus of 0.75 required more than twice the sodium oxide concentration to develop compressive strength in this range. All mixtures were workable with the exception of M_s=2.5 at 5 and 6% Na₂O. These strength values are neglected from the analysis.

These results suggest that a silica modulus of 2.5 is the most appropriate for sodium silicate-activated slag concrete, and that sodium oxide concentrations should be in the range of 1.5-4% by mass of slag. Within this range, mixtures develop strength of 30-40 MPa while remaining adequately workable. These conditions are attainable with lower silica moduli (0.75 and 1.5), but increased sodium oxide concentration is necessary. This is less desirable as it increases the environmental impact of the cement-free concrete.

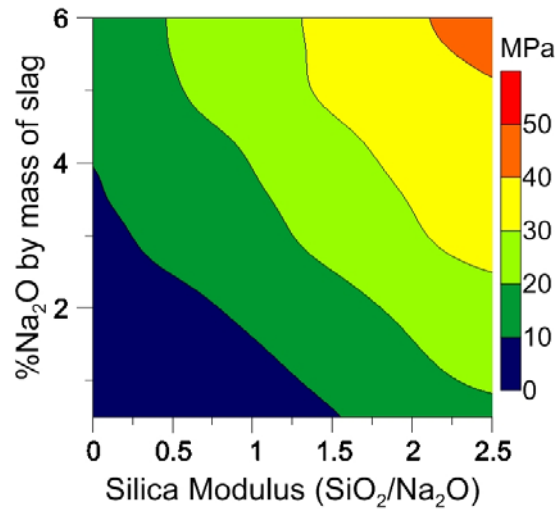


Figure 10: Contour plot of compressive strength of AAS concrete with varying silica modulus and sodium oxide concentration (50°C, 48 hr).

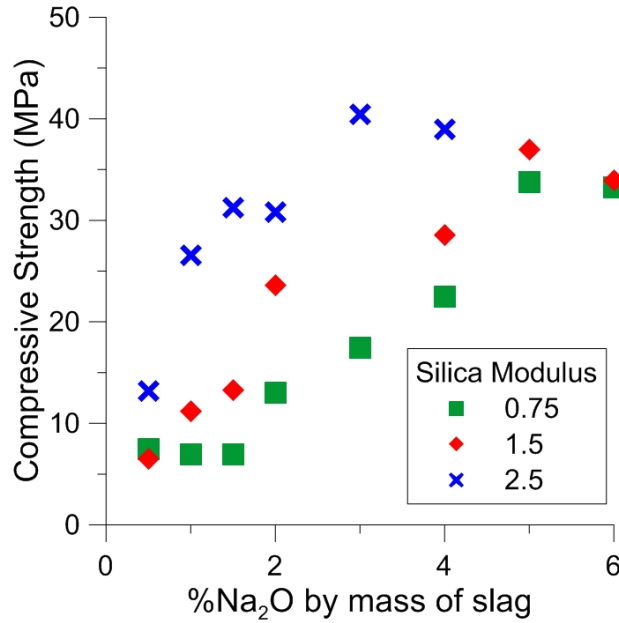


Figure 11: Compressive strength of AAS concrete with varying silica modulus and sodium oxide concentration (50°C, 48 hr).

3.1.5.2 Sodium Silicate-Activated Fly Ash

The compressive strength of AAF concrete with solution/binder ratio of 0.40, 0.1% AEA dosage by mass of fly ash, and cured at 50°C for 48 hours is plotted in Figures 12. The complete mixture proportions of all mixtures are listed in Table 13 in the appendices. The compressive strength of all mixtures was very low compared to AAS concretes, with a maximum strength of less than 30 MPa. The best performing mixtures were those with silica moduli of 1.0 and 1.5. A silica modulus of 2.0 resulted in acceptable strength, but workability in need of improvement. The compressive strength of these mixtures is plotted in Figure 13.

Even with relatively high sodium oxide concentration, these mixtures remained relatively weak. It is interesting to note that no appreciable strength was developed at either silica modulus until the sodium oxide concentration reached about 5%.

Previous researchers have seen significant strength development in AAF concrete at higher curing temperatures, so several of the same mixtures shown above with silica modulus of 1.5 were cast and cured for 48 hours at 75°C. The compressive strength of these mixtures is plotted in Figure 14. As with the mixtures cured at 50°C, the threshold for any strength development was approximately 5% Na₂O. At the elevated temperature, compressive strength of close to 40 MPa was developed with sodium oxide concentration of 5% and higher. Curing the same mixture at 50°C resulted in only about 10 MPa compressive strength.

These results show that AAF concrete requires curing at higher temperatures than slag in order to develop adequate strength. Nearly 30 MPa is attainable with 50°C curing, but only at very high sodium oxide concentration. At both temperatures, a minimum sodium oxide concentration for strength development of about 5% was identified, which can be identified on the contour plot previously presented in Figure 12. This behavior is in contrast with that of SS-Slag concrete, which shows a somewhat linear relationship between strength and sodium oxide concentration.

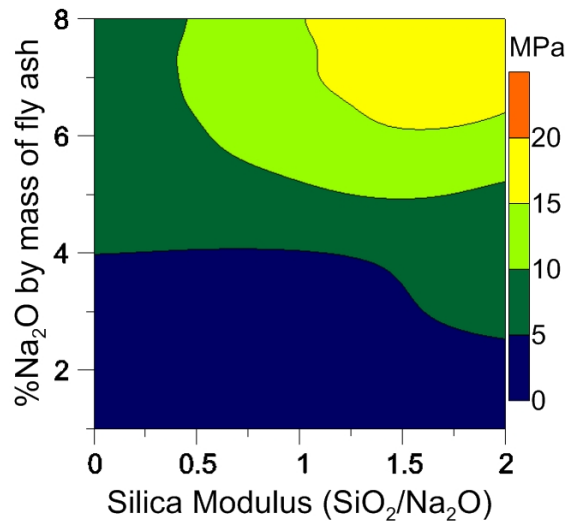


Figure 12: Contour plot of compressive strength of AAF concrete with varying silica modulus and sodium oxide concentration (50°C, 48 hr).

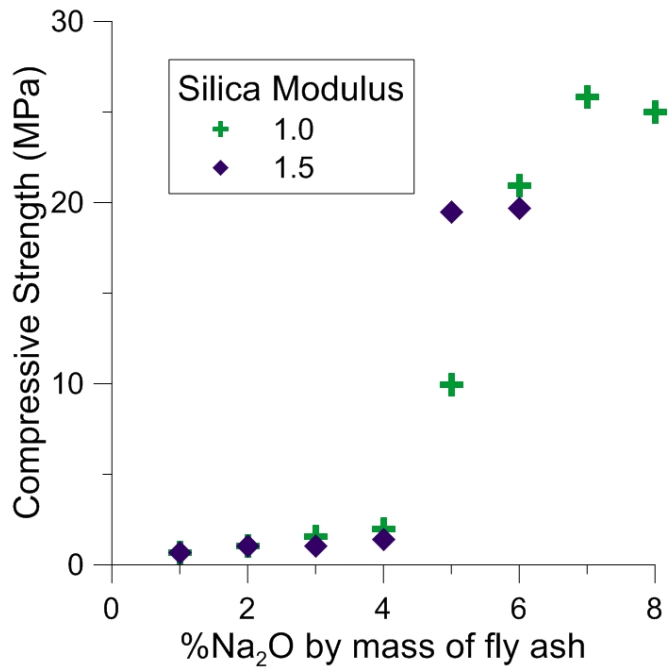


Figure 13: Compressive strength of AAF concrete with varying silica modulus and sodium oxide concentration (50°C, 48 hr).

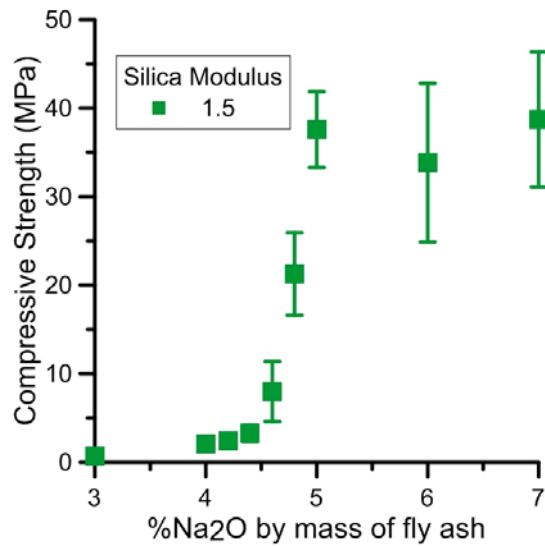


Figure 14: Compressive strength of AAF concrete with varying sodium oxide content (75°C, 48 hr).

3.1.6 Compressive Strength Modeling

Compressive strength modeling was performed based on the data from the previous section in order to provide a more full understanding of the effects of sodium oxide concentration and silica modulus on the compressive strength of AAC. Due to the low degrees of freedom, a low-order model was desirable. A multiple linear regression was selected of the form $Ax+By+C$, where x and y are the sodium oxide concentration and silica modulus, respectively, and the coefficients A , B , and C were selected to minimize the sum of the squared residuals.

The resulting model for AAS concrete is shown in Eq. 8, and is plotted in Fig. 15 for silica moduli between 0 and 2.5 and sodium oxide concentration between 0 and 6%. The details of the model are presented in Table 3, which includes the standard error and p-values for the model coefficients A , B , and C . P-values are a measure of the significance of the model, where a lower p-value indicates a more statistically significant fit. The minimum p-value is 0.0167, meaning that there is about a 1.67% chance that the model results could be explained by random variation. The coefficient of determination (R^2) for the AAS model is about 0.90. In order to demonstrate the goodness of fit, the model is plotted against the results for silica moduli of 0.75, 1.5, and 2.5 in Fig. 16. The figure shows reasonably good agreement with the compressive strength data with a few exceptions at very low and very high sodium oxide concentrations.

$$f_c = 11.67 \times M_s + 3.60 \times Na_2O - 5.55 \quad (8)$$

Table 3: Multiple linear regression model results for AAS concrete.

	Coefficient	p-value
M_s	11.67	1.25×10^{-11}
Na_2O %	3.60	6.96×10^{-8}
Intercept	-5.55	0.0161

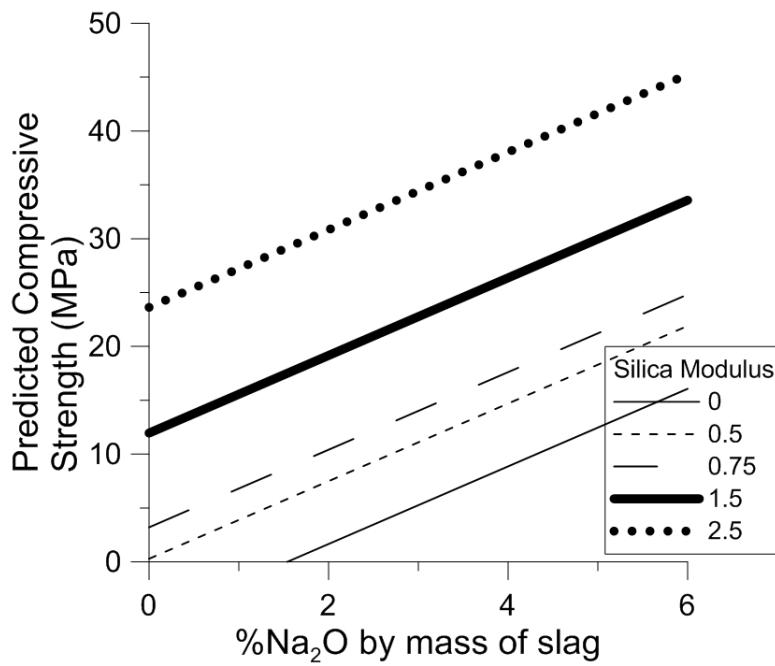


Figure 15: Multiple linear regression model results for AAS concrete with silica modulus between 0 and 2.5, and sodium oxide concentration between 0 and 6%.

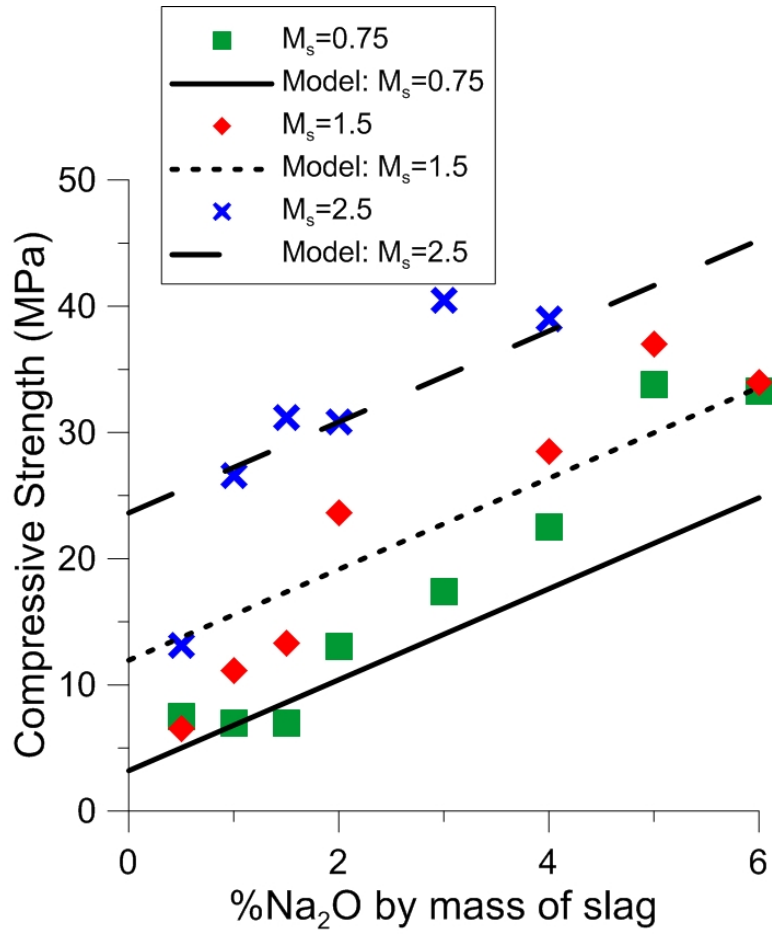


Figure 16: Comparison of multiple linear regression model and compressive strength data for selected AAS concrete mixtures.

Similarly, a model was proposed for AAF concrete mixtures. The resulting model is shown in Eq. 9 and is plotted in Fig. 17. The p-values for the model coefficients are included in Table 4, where it can be seen that the model for AAF concrete is only slightly less significant than that for AAS concrete, with about a 3% chance that the model results could be explained by random variation. However, the coefficient of determination (R^2) for the AAF model is only 0.65. The model is plotted with selected compressive strength data in Fig. 18, where it can be seen that, despite the low p-values, the fit is not very good. This is due to the non-linearity in the presented data as a result of the small working range of sodium oxide concentrations. AAF concrete only gained appreciable strength when sodium oxide concentration was at least 4.5%, and did not gain additional strength above 5%. Additional experimentation is necessary to more precisely identify this working range as well as the effect of silica modulus on this working range. At this time, additional modeling efforts are not useful due to the low sample size within the working range.

$$f'_c = 4.21 \times M_s + 2.17 \times Na_2O - 6.46 \quad (9)$$

Table 4: Multiple linear regression model results for AAF concrete.

	Coefficient	p-value
M_s	4.21	0.0098
Na_2O %	2.17	7.33×10^{-5}
Intercept	-6.46	0.0287

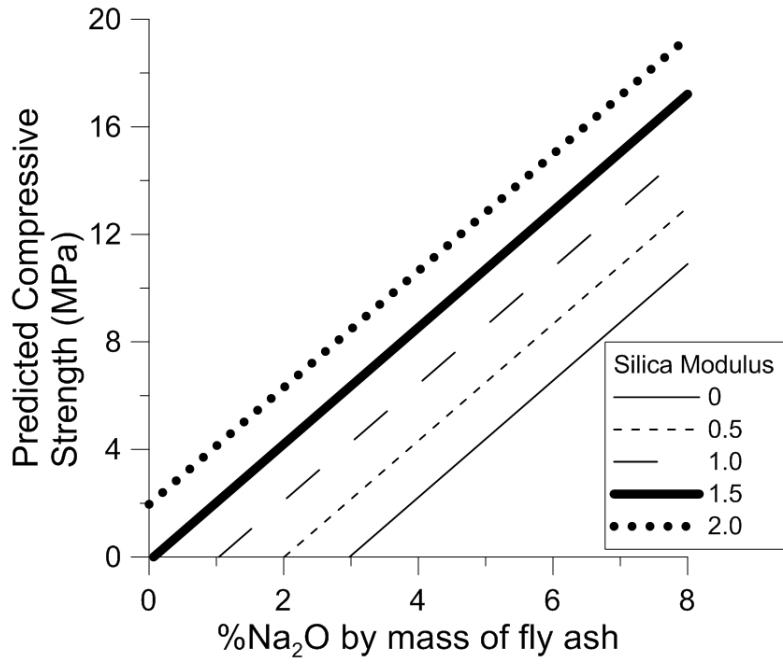


Figure 17: Multiple linear regression model results for AAF concrete with silica modulus between 0 and 2.5, and sodium oxide concentration between 0 and 6%.

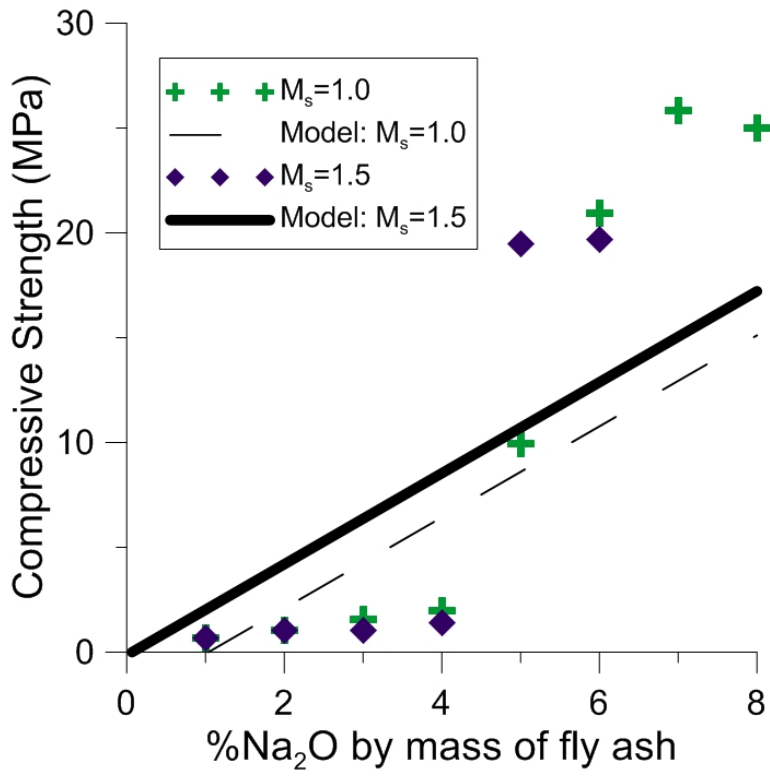


Figure 18: Comparison of multiple linear regression model and compressive strength data for selected AAF concrete mixtures.

3.1.7 Selection of Proposed Mixtures for In-Depth Study

Based on the preliminary work detailed in the above sections, four mixtures were selected for further investigation. These mixtures were those that were the most likely candidates for application in construction. Compressive strength was the most important consideration, and a target strength of at least 30 MPa was defined. Additionally, the mixtures had to be efficient. In this case, efficient mixtures were identified as those that had acceptable strength without the inclusion of very high alkali concentrations. For example, a mixture was inefficient if a similar strength could be achieved with a reduction in alkali, while an efficient mixture was one in which a reduction in alkalis led to a reduction in strength. Workability and setting time were also considered, but only to the extent that the mixtures had to be adequately workable to be easily cast without voids, honeycombs, flash setting, or segregation. It was assumed that these properties could be altered to some extent through the use of chemical admixtures during continued experimentation. Although no fly ash mixtures exhibited exemplary performance, for the sake of thoroughness, one fly ash mixture was selected. The remaining mixtures were slag with varying silica moduli and sodium oxide concentrations. The mixture parameters are included in Table 5.

Table 5: Optimal mixtures selected for in-depth analysis.

ID	s/b	Na ₂ O	M _s	SiO ₂	AEA	Coarse kg/m ³	Fine kg/m ³	Binder kg/m ³	Water kg/m ³	Na ₂ O	SiO ₂	AEA	fw/b
		%		%	%					kg/m ³	kg/m ³	kg/m ³	
S0	0.40	5.0	0.75	3.75	0.1	780	713.4	570	178.1	28.5	21.4	0.57	0.31
S1	0.40	5.0	1.5	7.5	0.1	780	713.4	570	156.7	28.5	42.8	0.57	0.27
S2	0.40	2.5	2.5	6.25	0.1	780	713.4	570	178.1	14.3	35.6	0.57	0.31
F1	0.40	5.0	1.5	7.5	0.1	780	638.7	570	156.7	28.5	42.8	0.57	0.27

3.2 Phase Two: Mechanical and Engineering Properties

The engineering properties, including elastic modulus, Poisson's ratio, compressive strength, and splitting tensile strength, of all four selected mixtures were evaluated for both ambient curing (22°C for 28 days) and elevated temperature curing (50°C for 48 hours). The results are presented in Table 6. The stress-strain curves for each mixture are plotted in Figs./ 19-26. Each plot shows two axial and lateral stress-strain curves within the elastic region as well as the axial stress-strain curve throughout the entire loading scheme, which is an average from two specimens. The former was used for the determination of the elastic modulus and Poisson's ratio in accordance with the specifications of ASTM C469.

Fig. 27 shows the splitting tensile strength of all mixtures as a function of the compressive strength. A least squares linear model is plotted in the figure. The model equation is presented in Eq. **Error! Reference source not found.** and has a coefficient of determination (R^2) of 0.99. The splitting tensile strength of OPC concrete is typically in the range of 10-15% of the compressive strength, while the results indicate that the splitting tensile strength of AAC is much higher at about 21% of the compressive strength. It is impossible to validate these conclusions due to the lack of relevant literature.

$$f_{sp} = 0.21 \times f'_c \quad (10)$$

The Poisson's ratio is essentially invariant for all of the mixtures tested here with a mean of 0.12 ± 0.003 . The typical value of Poisson's ratio expected for OPC concrete is 0.18-0.20. The observed value for the AAC mixtures presented here is 30-40% lower than this. This indicates that the lateral stiffness of AAC is high relative to that of OPC concrete. Practically, this means that the lateral tensile stresses developed in AAC are higher than those developed by OPC at the same lateral strain. This is consistent with the higher tensile strengths observed in AAC.

The elastic moduli of the AAC mixtures presented here were much lower than the expected values for OPC concrete. This is illustrated in Fig. 28, which shows the elastic moduli as a function of the compressive strengths. Also plotted in the figure are the elastic modulus equation from ACI-318 (normal strength concrete) and ACI-363 (high strength concrete) and the least squares linear model. As seen in the figure, both ACI equations overestimate the elastic modulus of AAC, in some cases by as much as 10-15 GPa. These results match the findings of other researchers who have similarly concluded that the elastic moduli of AAC are generally lower than those of OPC concrete [29, 46]. However, a simple least squares linear model was developed and fits the data very well. The model equation is presented in Eq. **Error! Reference source not found.** and has a coefficient of determination (R^2) of 0.95.

$$E = 600 \times f'_c \quad (11)$$

The stress-strain relationships included in Figs. 19-26 show the behavior of the AAC specimens under strain-controlled loading. The majority of specimens failed suddenly, brittlely, and in pure compression characterized by axial splitting. The brittle failure can be seen in many of the stress-strain curves, where the load reaches a maximum value, decreases slightly, and then fails completely. This has negative implications in terms of fracture toughness, since very little strain energy is absorbed after reaching the ultimate strength. Very brittle, explosive failure is typical of very high strength concrete, but is unusual for concrete in the strength range seen here. Typical stress-strain curves for normal strength concrete resemble those seen in Figs. 20 and 22, where the predominate behavior is strain softening. This is an indication that, in general, AAC exhibits much higher brittleness than typical of OPC concretes. This is potentially due to the higher tensile strength of the specimen, which allows for the development of higher strain energy prior to failure. When failure does occur the release of energy is much higher, hence the explosive failure mode.

Table 6: Engineering properties of sodium silicate-activated fly ash and slag concrete mixtures.

Mixture	Curing Condition	f'_c , MPa	f'_{sp} , MPa	E, GPa	μ
S0	22°C×28 d	29.9	6.9	21.7	0.123
S0	50°C×48 hr	37.3	7.3	26.7	0.126
S1	22°C×28 d	34.1	7.0	20.1	0.120
S1	50°C×48 hr	41.8	8.9	17.7	0.123
S2	22°C×28 d	37.3	9.2	27.9	0.121
S2	50°C×48 hr	41.6	7.9	17.0	0.122
F1	22°C×28 d	16.1	4.4	11.1	0.126
F1	50°C×48 hr	29.2	6.1	19.6	0.130

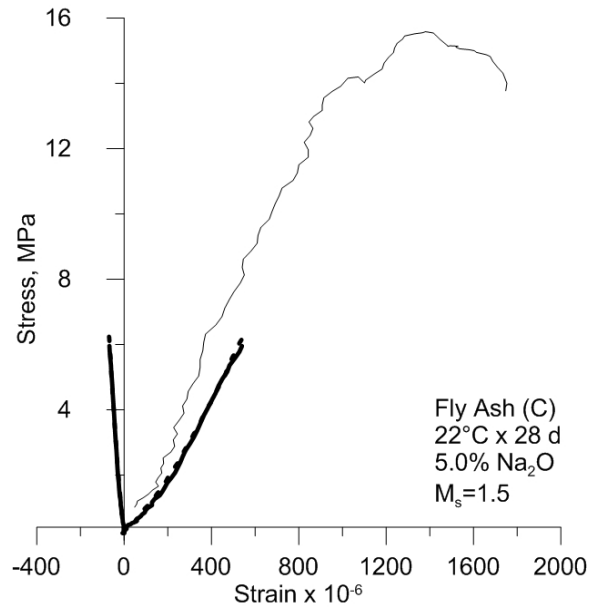


Figure 19: Stress-strain response for ambient temperature-cured fly ash F1 (5.0% Na₂O, M_s=1.5).

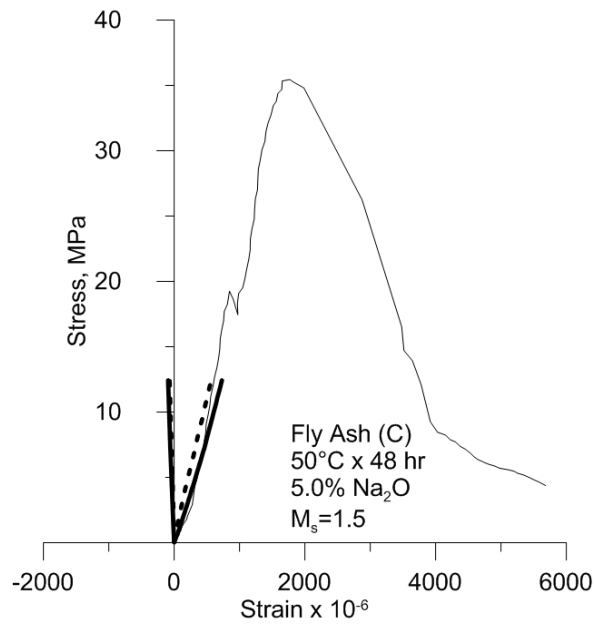


Figure 20: Stress-strain response for elevated temperature-cured fly ash F1 (5.0% Na₂O, M_s=1.5).

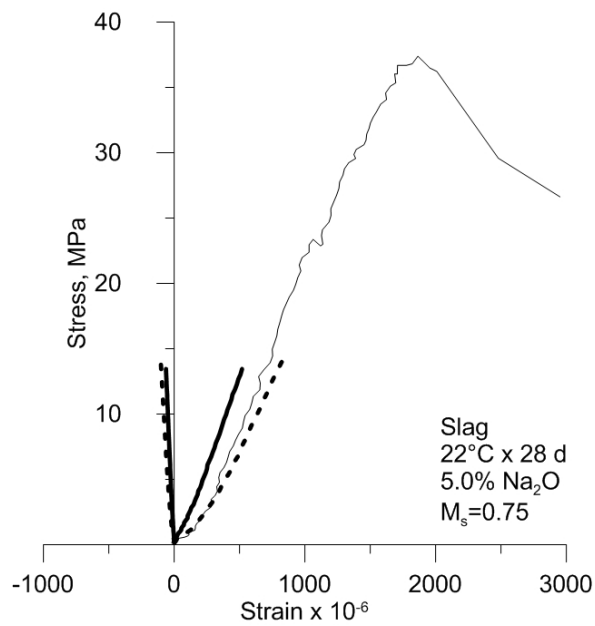


Figure 21: Stress-strain response for ambient temperature-cured slag S0 (5.0% Na₂O, M_s=0.75).

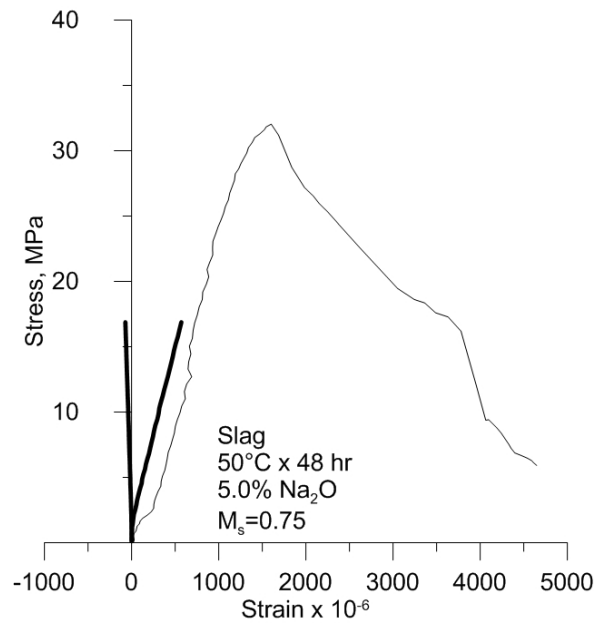


Figure 22: Stress-strain response for elevated temperature-cured slag S0 (5.0% Na₂O, M_s=0.75).

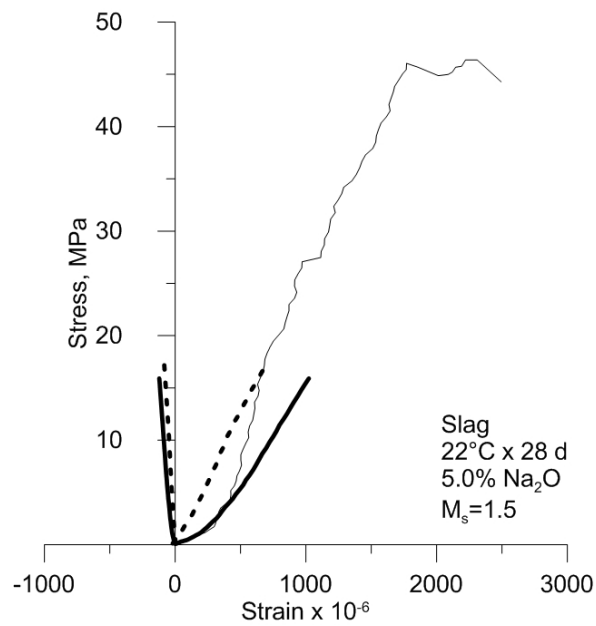


Figure 23: Stress-strain response for ambient temperature-cured slag S1 (5.0% Na₂O, M_s=1.5).

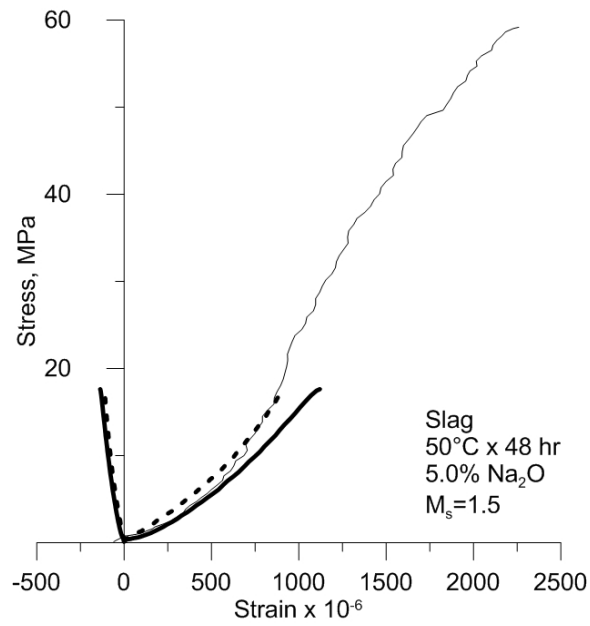


Figure 24: Stress-strain response for elevated temperature-cured slag S1 (5.0% Na₂O, M_s=1.5).

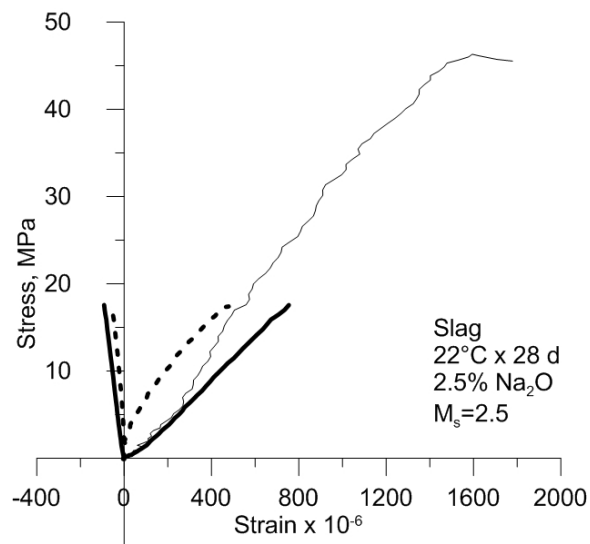


Figure 25: Stress-strain response for ambient temperature-cured slag S2 (2.5% Na₂O, M_s=2.5).

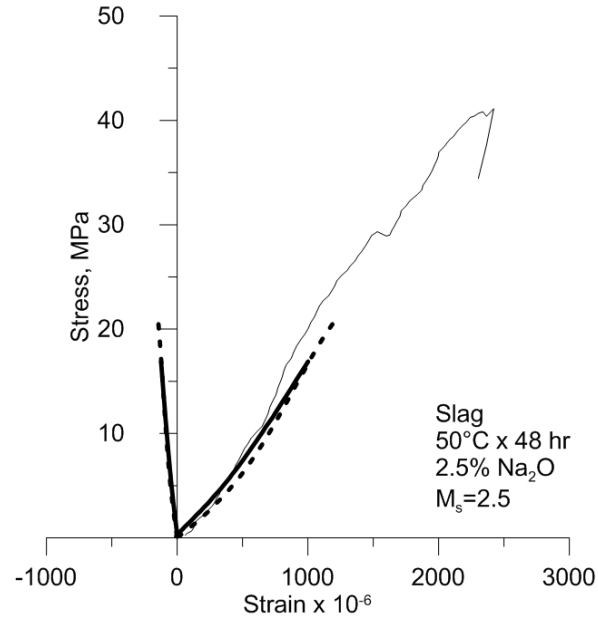


Figure 26: Stress-strain response for elevated temperature-cured slag S2 (2.5% Na₂O, M_s=2.5).

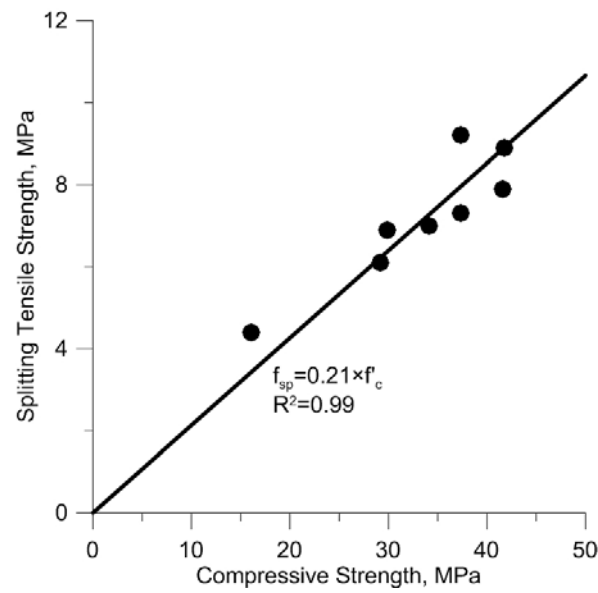


Figure 27: Splitting tensile strength of AAS and AAF concrete as a function of compressive strength.

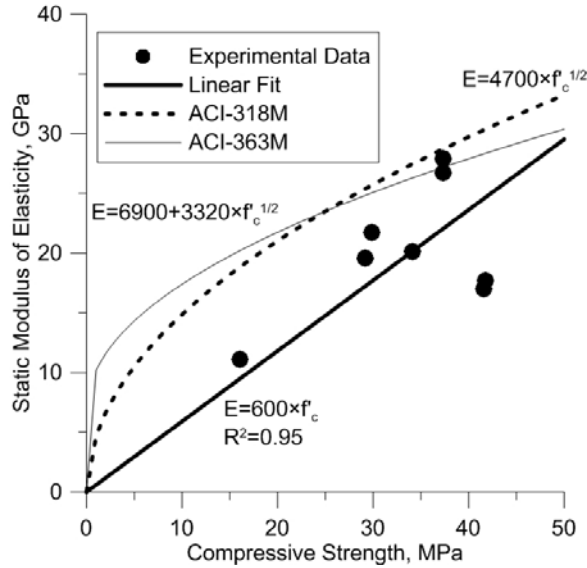


Figure 28: Elastic modulus of AAC mixtures as a function of compressive strength

3.3 Phase Three: Durability Properties

3.3.1 Drying Shrinkage

Drying shrinkage was evaluated for the proposed mixtures under two curing conditions: ambient temperature curing for 72 hours and elevated temperature curing at 50°C for 48 hours followed by 24 hours at ambient temperature. The resulting drying shrinkage strains are presented in Fig. 29, in which the square markers represent elevated temperature-cured specimens and the circular markers represent ambient temperature-cured specimens. Each curve represents the average shrinkage of at least two specimens.

As shown in the figure, the drying shrinkage strain observed in elevated temperature-cured specimens was significantly lower for all mixtures. This was likely due to excessive shrinkage during the elevated temperature curing process. Shrinkage during curing was not measured, but is identified as an area of future research. Cracking was observed in many of these specimens after removal from the curing environment, as shown in Fig. 30. These specimens were discarded. This shrinkage cracking could be a result of premature drying or could be due to high-magnitude autogenous shrinkage during the curing period. This is one area in which additional research is necessary.

The ambient temperature-cured specimens exhibited much higher-magnitude drying shrinkage strain than elevated temperature-cured specimens. The highest magnitude shrinkage was observed in the fly ash-based concrete, which also exhibited the most rapid shrinkage. The fly ash concrete developed over 2000 $\mu\sigma$ shrinkage in five days and reached steady state in under 30 days. In contrast, the slag concretes exhibited much more gradual shrinkage, reaching steady state after 50 to 60 days. The drying shrinkage in all slag mixtures had very similar trends, but the magnitude of the total shrinkage appeared to be inversely related to the silica modulus. This trend is more clearly seen in Fig. 31, which displays the drying shrinkage of ambient temperature-cured slag concretes only. However, the silica content ($M_s \times \%Na_2O$) of S1 (7.5% by mass of binder) is actually higher than that of S2 (6.25%), while the sodium oxide concentration of S2 is half that of S0 and S1. It is therefore evident that the drying shrinkage of sodium silicate-activated concrete varies inversely with silica content and varies directly with sodium oxide concentration.

With the exception of elevated temperature-cured mixtures which have previously been discussed, the drying shrinkage of the sodium silicate-activated concretes presented here are far in excess of those exhibited by typical OPC concretes. Typically observed values for drying shrinkage strain of OPC concrete are on the order of 500 $\mu\sigma$, while the shrinkage strains of the mixtures presented here were in the range of 1000-2500 $\mu\sigma$. Evidence does exist in the literature that shrinkage-reducing admixtures are effective at reducing the drying and autogenous shrinkage of alkali-activated concretes [41], and as such the authors of the current study have identified this as an area in need of further research.

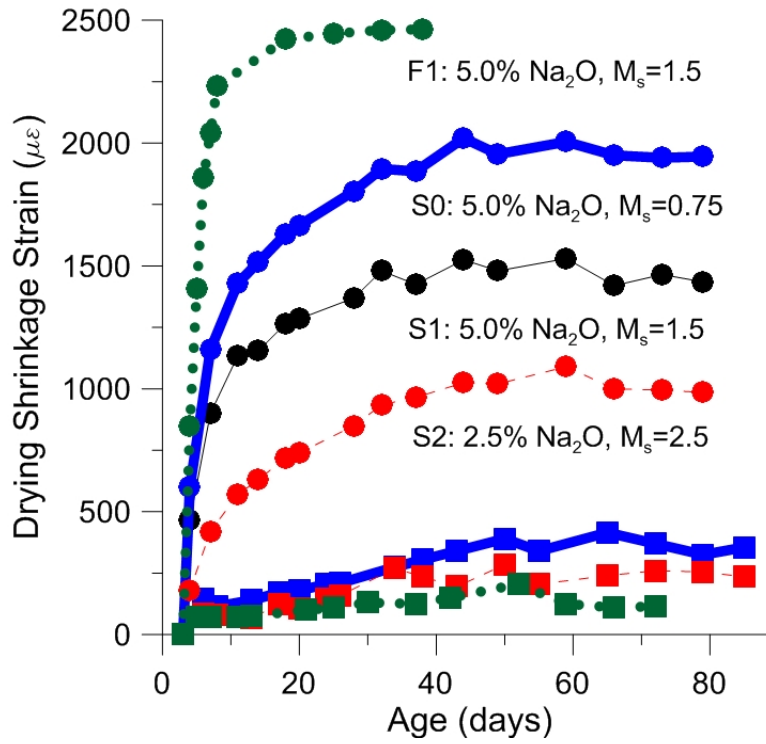


Figure 29: Drying shrinkage strain of alkali-activated fly ash (C) and slag concrete stored at 50%RH.



Figure 30: Shrinkage cracking in sodium silicate-activated fly ash concrete cured at elevated temperature (50°C for 48 hours).

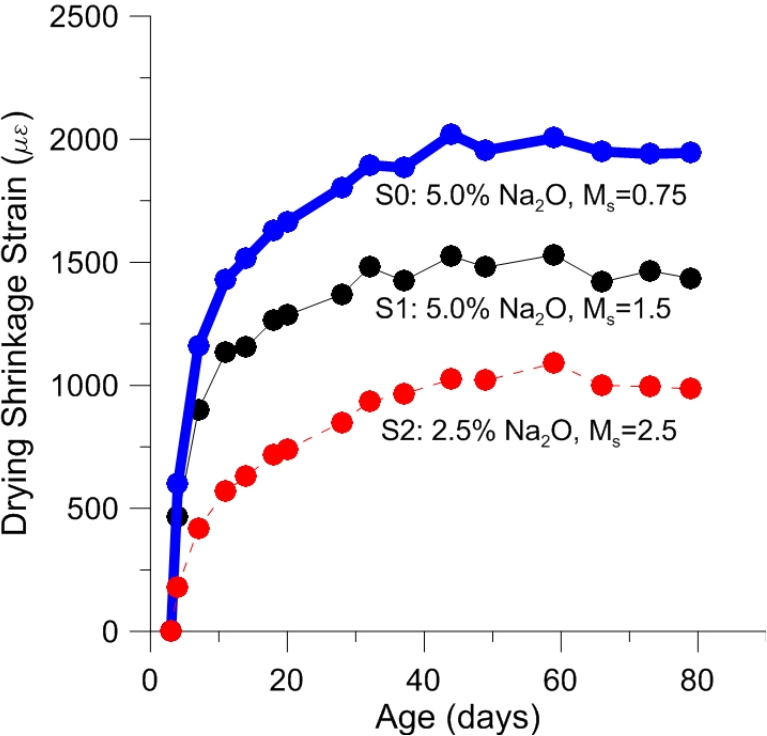


Figure 31: Drying shrinkage strain of slag concrete mixtures cured at ambient temperature (22°C for 72 hours). Activator concentrations are reported relative to the mass of binder.

3.3.2 Alkali-Silica Reaction Potential

Alkali-silica reaction potential was measured using both the slow method (ASTM C227) and the accelerated method (ASTM C1567) for all four selected mixtures. For the slow method, mortar bars were cast using both normal and alkali-reactive aggregate. The resulting 14-day expansion is plotted in Fig. 32 as the average expansion of three mortar bars tested simultaneously. Mixtures S0 and S1 showed positive expansion with both normal and alkali-reactive aggregate. Interestingly, the expansion was less for mortar bars cast with aggregate that is known to cause deleterious expansion in OPC systems. Mixture S0 with normal aggregate exhibited particularly high expansion of nearly 0.35% in 14 days. It was also interesting that several of the mixtures actually exhibited shrinkage during the ASR testing, despite the fact that the high-humidity, high-temperature test conditions were designed to promote expansion. This is likely an additional indicator that shrinkage is a significant issue for AAC.

The expansion of mortar bars during the accelerated test method is plotted in Fig. 33, which displays the average expansion of four specimens from each mixture tested simultaneously. This test gave more satisfying results, as all specimens underwent expansion due to the immersion in sodium hydroxide. Since the expansion of specimens containing normal aggregate was at least as high as that of specimens containing alkali-reactive aggregate for the slow test method, only normal aggregate was used for the accelerated test method. The accelerated test method resulted in positive expansion for all mixtures, as seen in the figure. Mixture S1 (5% Na₂O, M_s=1.5) exhibited the lowest expansion of about 0.1% after 14 days exposure to the sodium hydroxide solution. The fly ash mixture, having the same solution concentrations, exhibited only slightly higher expansion. This indicates that fly ash (C) has higher ASR potential than slag. Mixtures S1 (5% Na₂O, M_s=1.5) and S2 (2.5% Na₂O, M_s=2.5) exhibited very high expansion, nearing 0.5% and 1%, respectively, in 14 days.

Little correlation was seen between the results of the two ASR test methods. Mixture S1 exhibited relatively high expansion in both tests, but mixture S2 exhibited the highest expansion during the accelerated testing while exhibiting shrinkage during the slow test method. Both the Federal Highway Administration (FHWA) and the National Ready Mix Concrete Association (NRMCA) classify systems as non-reactive when the expansion is less than 0.04% in one year under test conditions prescribed by ASTM C1293, which involves the long-term storage of concrete prisms in water at 38°C. Neither test method employed here is exactly analogous to this method due to the time required to perform ASTM C1293. However, the expansion of the majority of specimens exceeded the value of 0.04% in only 14 days. This indicates that alkali-silica reaction is a potential problem in AAC systems, despite available literature indicating otherwise [22, 33, 36-38]. This could potentially be due to differences in the chemical and physical properties of the aggregate, which could be verified by additional testing. Although it was not possible due to the time constraints of this study, long-term testing should be performed according to ASTM C1293 in order to allow for more precise comparison with transportation industry standards. Additionally, more information regarding the effect of mixture parameters on the ASR expansion would be useful in formulating more effective AAC mixtures.

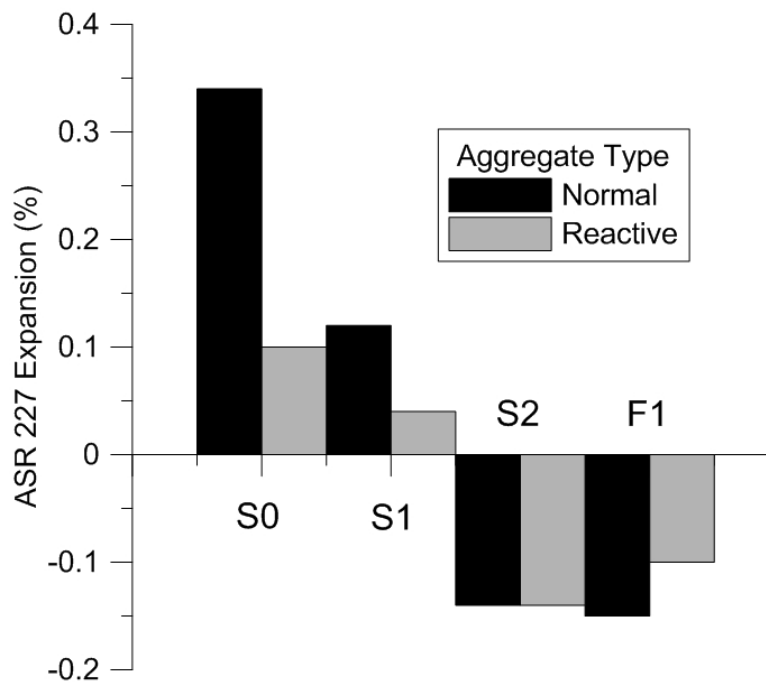


Figure 32: ASR expansion measured during ASTM C227 testing. Positive values indicate expansion.

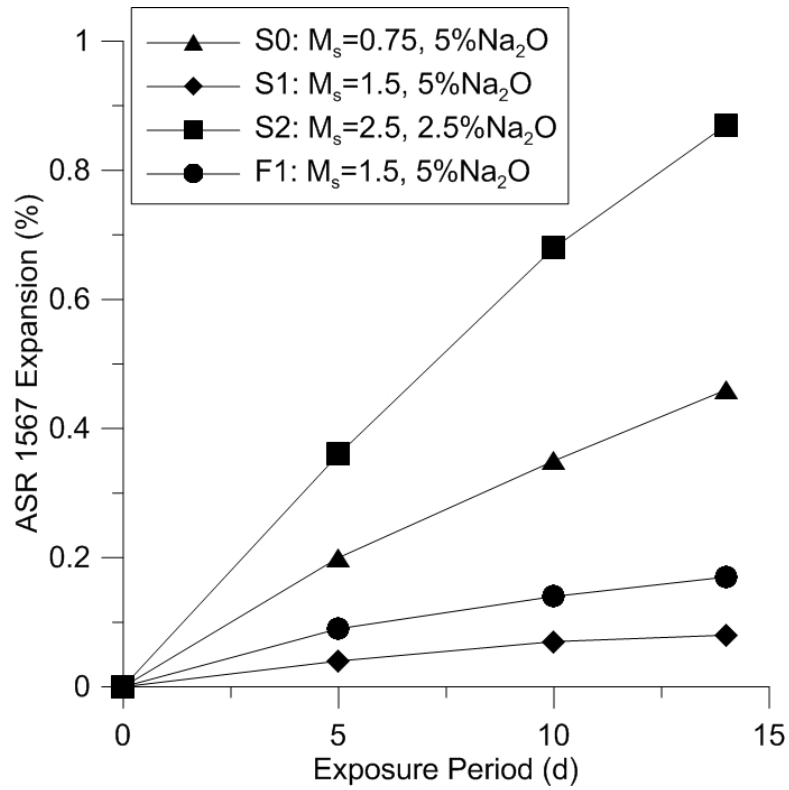


Figure 33: ASR expansion measured during ASTM C1567 accelerated testing. Positive values indicate expansion.

3.3.3 Chloride Ion Penetrability

RCPT was performed on two specimens from each mixture for both ambient and elevated temperature curing conditions. The results are displayed in Fig. 34 as the average charge passed (C) for two specimens over the six-hour test period. For three specimen groups (S1 at ambient temperature, and F1 at both ambient and elevated temperature), the test resulted in an error. This occurs only when the instantaneous current exceeds 500 mA during the test cycle. Since charge is the product of current and time, the charge passed when the current exceeds this value is in excess of 10,000 C. Therefore, the value of 10,000 C is tentatively reported for these specimen groups. It is difficult to draw specific conclusions from these tests, although it is apparent that the fly ash mixture is highly susceptible to chloride ion ingress, as is the slag mixture S1 with silica modulus 1.5 and 5% sodium oxide content. Mixture S1 also had very high chloride ion penetrability when cured at elevated temperature.

The RCPT results for the remaining mixtures varied widely. The best performing mixtures were S0 and S2, although the permeability of these specimens was classified as moderate based on the specification of ASTM C1202. The majority of specimens were classified as highly permeable (greater than 4000 C charge passed). No pattern is apparent with regard to the effect of elevated temperature curing on the chloride penetrability of the concrete. However, the chloride ion penetrability of all mixtures tested here (with the potential exception on mixture S0 at elevated temperature curing) is higher than would be acceptable for transportation infrastructure which commonly sees high chloride exposure.

It was noted that the temperature in many of the tests exceeded 40°C. As concluded by a few other studies, this is one fundamental issue with RCPT [47]. The current applied to the specimens increases the temperature. As the temperature rises, the resistance to chloride ion diffusion is greatly reduced, which causes the current flow to increase. This can continue in succession. Additionally, there is concern regarding the specimen preparation method. The authors have previously concluded that there is a high prevalence of microcracking in AAC, particularly when subjected to mechanical damage such as cutting. Although an effort was made to reduce this damage during the preparation of RCPT cylinders by cutting slowly and with plenty of cooling water, this could potentially increase the chloride penetrability.

The chloride penetrability is a very important property with regard to the durability of transportation structures. It is recommended that further research be performed in this area in order to develop a more complete understanding of how AAC mixture parameters influence permeability and chloride ion penetrability. Further RCPT investigations should be performed, but with a modified technique. This could include a reduction in the applied voltage in order to reduce heat buildup. Disk specimens could also be individually molded and polished rather than being cut from cylinders to avoid microcracking due to the cutting process. In addition to modified RCPT, alternative evaluation techniques should be employed, including salt ponding (ASTM C1543), non-steady state chloride migration, and electrical resistivity methods.

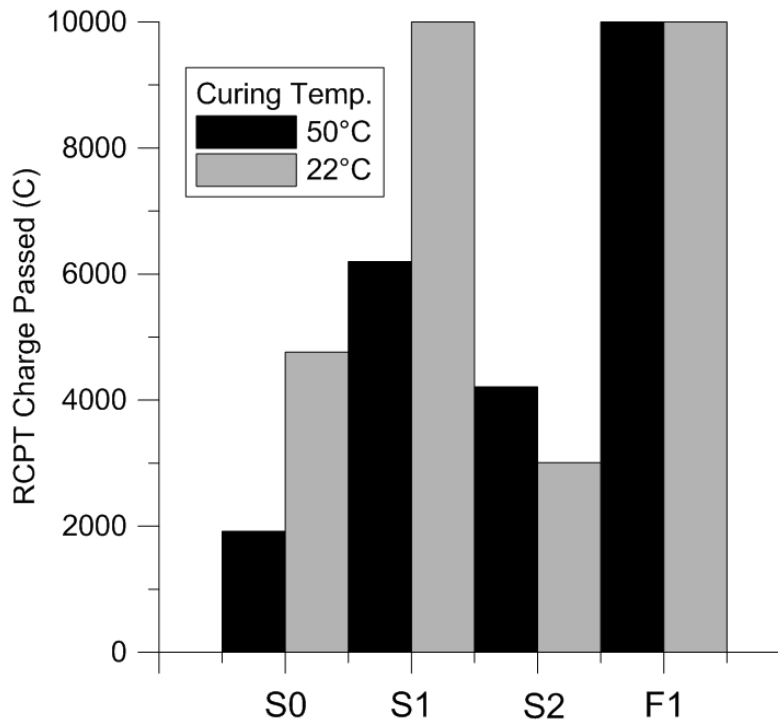


Figure 34: Charge passed (C) during six-hour duration of RCPT.

4 Conclusions and Recommendations

The following conclusions were drawn from the results and discussion presented above:

1. **AAS and AAF concretes were developed having strength in the range of 30-40 MPa.**

However, several issues remain regarding the practicality of these mixtures. Workability and

setting time are of concern since the mixtures tend to set rapidly, particularly in the case of fly ash. In general, slag mixtures perform better in terms of both strength and workability. Compressive strength is much more sensitive to activator concentrations than to water content.

2. **Minimal additions of AEA (0.1% by mass of binder) greatly improve the workability of AAC mixtures.** Compressive strength increases are noted with additions of AEA due to improved consolidation, particularly in very harsh mixtures with high activator concentration or low water content.
3. **Elevated temperature curing at 50°C for 48 hours provides nearly identical strength to 28-day ambient temperature curing.** Curing for additional time at elevated temperature does not seem to increase the compressive strength, but increasing the temperature to 75°C results in a significant strength increase.
4. **Multiple linear regression models have been proposed correlating the compressive strength of AAS and AAF concrete to the concentration of sodium oxide and silica in the activator solution.** The AAS model fits the experimental data very well and is an accurate predictor of compressive strength. However, the AAF model fits the experimental data poorly; this is a result of the limited working range of activator concentrations that results in adequately workable AAF mixtures.
5. **The tensile strength of AAC mixtures were shown to be approximately 21% of the compressive strength and the Poisson's ratio was most nearly 0.12 for all mixtures.** In OPC systems, the tensile strength is typically 10-15% of the compressive strength and the Poisson's ratio is typically 0.18. This means that AAC shows increased lateral stiffness when compared to typical OPC concrete.
6. **The elastic moduli of AAS and AAF concretes was shown to be about 600 times the compressive strength.** The ACI approximation for elastic modulus of OPC concrete, which is proportional to the square root of the compressive strength, overestimates the modulus of AAC by as much as 10-15 GPa. In general, the axial stiffness of AAC is much less than that expected of OPC concrete with similar strength. Elastic moduli were observed in the range of 10-25 GPa.

7. **AAC exhibits highly brittle stress-strain behavior.** The brittleness of the majority of specimens tested showed brittle behavior similar to high-strength OPC concrete, despite relatively low compressive strengths. This implies that the fracture toughness of AAC may be much lower than that of comparable OPC concrete.
8. **Despite available literature indicating the contrary, several mixtures have exhibited unacceptable expansion due to ASR.** However, ASR expansion results from two different methods showed no correlation with one another. Additionally, some specimens actually exhibited shrinkage under conditions designed to amplify ASR expansion. As such, no specific conclusions could be drawn with regard to ASR.
9. **The permeability of AAC is of potential concern.** RCPT results indicated very high permeability in most mixtures tested here. However, literature indicates that there are potential issues regarding the use of RCPT as a method of evaluating the permeability of AAC. Alternative methods may be more applicable, as discussed below.
10. **AAC mixtures exhibit high-magnitude drying shrinkage.** The drying shrinkage of ambient temperature-cured AAC mixtures ranged from 1000-2500 $\mu\epsilon$ within 30 days, which is unacceptably high. The drying shrinkage of elevated temperature-cured specimens was significantly lower, although it is likely that these specimens experienced shrinkage during the curing process.
11. **The mixtures proposed in this study are can not currently be put into practical use.** This is predominately due to the uncertainty surrounding the durability issues and the limited workability of the mixtures. Further research into the durability properties and methods of improving workability are necessary to make the proposed mixtures practice-ready. This is discussed in detail below.

The authors have identified the following areas which are in need of further research in order to fully characterize the behavior of AAC and evaluate its appropriateness for bridge deck and pavement applications:

1. **Detailed investigation into drying and autogenous shrinkage.** It has been shown that the proposed mixtures are highly sensitive to drying shrinkage, and has been suggested that autogenous shrinkage is also of high concern. Some mixtures exhibited shrinkage even at very high relative humidity during ASR (ASTM C227) testing. Further research is necessary

to explain this behavior. This effort should include evaluation of the effect of various chemical and mineral admixtures on shrinkage in order to identify appropriate methods of shrinkage mitigation.

2. **Validation and continuation of ASR evaluation.** Two methods of evaluation of ASR expansion were employed in this study, but trends were not evident in the results from either method. Experiments should be carefully repeated in order to validate the current results. Additional test methods should be employed, including long-term methods (ASTM C1260) referenced by FHWA and NRMCA.
3. **Further investigation into permeability.** The RCPT results presented here indicate impractically high permeability in AAC. However, this is likely due to the chemistry of the pore solution rather than the microstructure of the concrete. More appropriate methods of permeability assessment should be employed, including electrical impedance techniques, mercury intrusion porosimetry, microstructural characterization, and modified RCPT with reduced voltage.
4. **Continuation of compressive strength modeling.** Preliminary relationships have been proposed for compressive strength as a function of alkali concentrations. The relationship proposed for AAS concrete fits experimental data reasonably well. However, the model proposed for AAF concrete is a poor fit. This is likely due to the limited working range of sodium oxide concentration (4-8%). Additional data is necessary to validate this claim, and further modeling efforts are required to find a more appropriate representation of the material behavior.
5. **Quantitative evaluation of workability and setting time.** The workability and setting time of mixtures presented in this study were only coarsely observed and classified based on the ability to cast and consolidate specimens. Quantitative analysis of these properties and the effect of various chemical and mineral admixtures is necessary for practice-readiness.
6. **Continuation of engineering property investigation.** Relatively little information is available regarding the engineering properties of AAC. Further investigation is necessary to provide information on the effect of mixture parameters, curing conditions, and maturity on engineering properties. Additionally, much more data is necessary to determine the relationship between compressive strength and elastic modulus in AAC.

5 Publication

A portion of the information presented here has been published in the conference proceedings of and presented in poster form at the Transportation Research Board 2014 Annual Meeting. Work was presented under the title "Alkali-Activated Cement Free Concrete: Development of Practical Mixtures for Construction," paper no. 14-4674. We are also preparing a full length research paper manuscript that will be submitted for possible publication in ACI Materials

References

- [1] Hendrik G van Oss. Cement. *United States Geological Survey (USGS) minerals yearbook: cement*, 2011.
- [2] P Kumar Mehta. Reducing the environmental impact of concrete. *Concrete International*, 23(10):61–66, 2001.
- [3] Ernst Worrell, Lynn Price, Nathan Martin, Chris Hendricks, and Leticia Ozawa Meida. Carbon dioxide emission from the global cement industry. *Annual Review of Energy and the Environment*, 2001.
- [4] MA Smith and GJ Osborne. Slag/fly ash cements. *World Cement Technology*, 8(6), 1977.
- [5] FJ Hogan and JW Meusel. Evaluation for durability and strength development of a ground granulated blast furnace slag. *Cement, Concrete and Aggregates*, 3(1), 1981.
- [6] Richard Helmuth. *Fly ash in cement and concrete*. Number SP040. 01T. 1987.
- [7] VM Malhotra. Fly ash, slag, silica fume, and rice-husk ash in concrete: a review. *Concrete International*, 15:23–23, 1993.
- [8] EE Berry and V Mohan Malhotra. Fly ash for use in concrete—a critical review. In *ACI Journal Proceedings*, volume 77. ACI, 1980.
- [9] Bryan K Marsh and Robert L Day. Pozzolanic and cementitious reactions of fly ash in blended cement pastes. *Cement and Concrete Research*, 18(2):301–310, 1988.
- [10] YUAN RUNZHANG, GAO QIONGYING, and OUYANG SHIXI. Study on structure and latent hydraulic activity of slag and its activation mechanism. *Silicates industriels*, 53(3-4):55–59, 1988.
- [11] SC Pal, A Mukherjee, and SR Pathak. Investigation of hydraulic activity of ground granulated blast furnace slag in concrete. *Cement and Concrete Research*, 33(9):1481–1486, 2003.
- [12] A Palomo, MW Grutzeck, and MT Blanco. Alkali-activated fly ashes: a cement for the future. *Cement and Concrete Research*, 29(8):1323–1329, 1999.
- [13] Norihiro Murayama, Hideki Yamamoto, and Junji Shibata. Mechanism of zeolite synthesis from coal fly ash by alkali hydrothermal reaction. *International Journal of Mineral Processing*, 64(1):1–17, 2002.
- [14] Ana Fernández-Jiménez and A Palomo. Composition and microstructure of alkali activated fly ash binder: effect of the activator. *Cement and Concrete Research*, 35(10):1984–1992, 2005.
- [15] M Criado, Ana Fernández-Jiménez, and A Palomo. Alkali activation of fly ash: Effect of the $\text{SiO}_2/\text{Na}_2\text{O}$ ratio: Part I: FTIR study. *Microporous and mesoporous materials*, 106(1):180–191, 2007.
- [16] Shao-Dong Wang, Karen L Scrivener, and PL Pratt. Factors affecting the strength of alkali-activated slag. *Cement and concrete research*, 24(6):1033–1043, 1994.
- [17] FG Collins and JG Sanjayan. Workability and mechanical properties of alkali activated slag concrete. *Cement and concrete research*, 29(3):455–458, 1999.
- [18] B Talling and J Brandstetr. Present state and future of alkali-activated slag concretes. *ACI Special Publication*, 114, 1989.
- [19] C Shi and RL Day. Selectivity of alkaline activators for the activation of slags. *Cement, Concrete and Aggregates*, 18(1), 1996.

- [20]T Bakharev, JG Sanjayan, and Y-B Cheng. Effect of elevated temperature curing on properties of alkali-activated slag concrete. *Cement and concrete research*, 29(10):1619–1625, 1999.
- [21]Chunming Gong and Nanru Yang. Effect of phosphate on the hydration of alkali-activated red mud–slag cementitious material. *Cement and Concrete Research*, 30(7):1013–1016, 2000.
- [22]F Puertas, S Martí nez-Rami ñ rez, S Alonso, and T Vazquez. Alkali-activated fly ash/slag cements: strength behaviour and hydration products. *Cement and Concrete Research*, 30(10):1625–1632, 2000.
- [23]Frank Collins and JG Sanjayan. Microcracking and strength development of alkali activated slag concrete. *Cement and Concrete Composites*, 23(4):345–352, 2001.
- [24]Ana Fernández-Jiménez, F Puertas, et al. Effect of activator mix on the hydration and strength behaviour of alkali-activated slag cements. *Advances in cement research*, 15(3):129–136, 2003.
- [25]AR Brough and A Atkinson. Sodium silicate-based, alkali-activated slag mortars: Part i. strength, hydration and microstructure. *Cement and Concrete Research*, 32(6):865–879, 2002.
- [26]E Douglas, A Bilodeau, J Brandstetr, and VM Malhotra. Alkali activated ground granulated blast-furnace slag concrete: preliminary investigation. *Cement and concrete research*, 21(1):101–108, 1991.
- [27]E Douglas, A Bilodeau, and VM Malhotra. Properties and durability of alkali-activated slag concrete. *ACI Materials Journal*, 89(5), 1992.
- [28]T Bakharev, JG Sanjayan, and Y-B Cheng. Effect of elevated temperature curing on properties of alkali-activated slag concrete. *Cement and concrete research*, 29(10):1619–1625, 1999.
- [29]Ana M Fernandez-Jimenez, Angel Palomo, and Cecilio Lopez-Hombrados. Engineering properties of alkali-activated fly ash concrete. *ACI Materials Journal*, 103(2), 2006.
- [30]K Byfors, G Klingstedt, V Lehtonen, H Pyy, and L Romben. Durability of concrete made with alkali-activated slag. *ACI Special Publication*, 114, 1989.
- [31]Deepak Ravikumar and Narayanan Neithalath. Electrically induced chloride ion transport in alkali activated slag concretes and the influence of microstructure. *Cement and Concrete Research*, 47:31–42, 2013.
- [32]T Bakharev, J.G Sanjayan, and Y.-B Cheng. Resistance of alkali-activated slag concrete to acid attack. *Cement and Concrete Research*, 33(10):1607 – 1611, 2003.
- [33]Ana Fernández-Jiménez, I Garcia-Lodeiro, and A Palomo. Durability of alkali-activated fly ash cementitious materials. *Journal of materials science*, 42(9):3055–3065, 2007.
- [34]MAM Ariffin, MAR Bhutta, MW Hussin, M Mohd Tahir, and Nor Aziah. Sulfuric acid resistance of blended ash geopolymer concrete. *Construction and Building Materials*, 43:80–86, 2013.
- [35]Shane Donatello, Angel Palomo, and Ana Fernández-Jiménez. Durability of very high volume fly ash cement pastes and mortars in aggressive solutions. *Cement and Concrete Composites*, 38:12–20, 2013.
- [36]PM Gifford and JE Gillott. Alkali-silica reaction (asr) and alkali-carbonate reaction (acr) in activated blast furnace slag cement (abfsc) concrete. *Cement and concrete research*, 26(1):21–26, 1996.
- [37]Ana Fernández-Jiménez and F Puertas. The alkali–silica reaction in alkali-activated granulated slag mortars with reactive aggregate. *Cement and concrete research*, 32(7):1019–1024, 2002.
- [38]I García-Lodeiro, A Palomo, and Ana Fernández-Jiménez. Alkali–aggregate reaction in activated fly ash systems. *Cement and Concrete Research*, 37(2):175–183, 2007.

- [39] Yawei Fu, Liangcai Cai, and Wu Yonggen. Freeze–thaw cycle test and damage mechanics models of alkali-activated slag concrete. *Construction and Building Materials*, 25(7):3144–3148, 2011.
- [40] Shao-Dong Wang, Xin-Cheng Pu, KL Scrivener, and PL Pratt. Alkali-activated slag cement and concrete: a review of properties and problems. *Advances in cement research*, 7(27):93–102, 1995.
- [41] T Bakharev, JG Sanjayan, and Y-B Cheng. Effect of admixtures on properties of alkali-activated slag concrete. *Cement and Concrete Research*, 30(9):1367–1374, 2000.
- [42] Cengiz Duran Atiş, Cahit Bilim, Özlem Çelik, and Okan Karahan. Influence of activator on the strength and drying shrinkage of alkali-activated slag mortar. *Construction and building materials*, 23(1):548–555, 2009.
- [43] Adrian Pauw. Static modulus of elasticity of concrete as affected by density. In *ACI Journal Proceedings*, volume 57. ACI, 1960.
- [44] Ramon L Carrasquillo and Arthur H Nilson. Properties of high strength concrete subject to short-term loads. In *ACI Journal Proceedings*, volume 78. ACI, 1981.
- [45] PC Aitcin and PK Mehta. Effect of coarse aggregate characteristics on mechanical properties of high-strength concrete. *ACI Materials Journal*, 87(2), 1990.
- [46] RN Swamy and Ammar Bouikni. Some engineering properties of slag concrete as influenced by mix proportioning and curing. *ACI Materials Journal*, 87(3), 1990.
- [47] Caijun Shi. Strength, pore structure and permeability of alkali-activated slag mortars. *Cement and Concrete Research*, 26(12):1789–1799, 1996.
- [48] Saud Al-Otaibi. Durability of concrete incorporating ggbs activated by water-glass. *Construction and Building Materials*, 22(10):2059–2067, 2008.
- [49] Susan A Bernal, Ruby Mejía de Gutiérrez, Alba L Pedraza, John L Provis, Erich D Rodriguez, and Silvio Delvasto. Effect of binder content on the performance of alkali-activated slag concretes. *Cement and Concrete Research*, 41(1):1–8, 2011.
- [50] Deepak Ravikumar and Narayanan Neithalath. An electrical impedance investigation into the chloride ion transport resistance of alkali silicate powder activated slag concretes. *Cement and Concrete Composites*, 2013.
- [51] Velu Saraswathy and Ha-Won Song. Electrochemical studies on the corrosion performance of steel embedded in activated fly ash blended concrete. *Electrochimica acta*, 51(22):4601–4611, 2006.
- [52] Lewis H Tuthill. Alkali-silica reaction-40. *Concrete International*, 1982.
- [53] Medhat H Shehata and Michael DA Thomas. The effect of fly ash composition on the expansion of concrete due to alkali–silica reaction. *Cement and Concrete Research*, 30(7):1063–1072, 2000.
- [54] DW Hobbs. The effectiveness of pfa in reducing the risk of cracking due to asr in concretes containing cristobalite. *Magazine of Concrete Research*, 46(168):167–175, 1994.
- [55] Roy W Carlson. Drying shrinkage of large concrete members. In *ACI Journal Proceedings*, volume 33. ACI, 1937.
- [56] Povindar K Mehta. Concrete. structure, properties and materials. 1986.
- [57] Will Hansen. Drying shrinkage mechanisms in portland cement paste. *Journal of the American Ceramic society*, 70(5):323–328, 1987.

- [58] Benoît Bissonnette, Pascale Pierre, and Michel Pigeon. Influence of key parameters on drying shrinkage of cementitious materials. *Cement and Concrete Research*, 29(10):1655–1662, 1999.
- [59] David W Mokarem. *Development of concrete shrinkage performance specifications*. PhD thesis, Virginia Polytechnic Institute and State University, 2002.
- [60] S Tangtermsirikul. Class c fly ash as a shrinkage reducer for cement paste. *ACI Special Publication*, 153, 1995.
- [61] MN Haque. Strength development and drying shrinkage of high-strength concretes. *Cement and Concrete Composites*, 18(5):333–342, 1996.
- [62] NS Berke, MP Dallaire, MC Hicks, and A Kerkar. New developments in shrinkage-reducing admixtures. *ACI Special Publication*, 173, 1997.
- [63] Aleksandra Radlinska, Farshad Rajabipour, Brooks Bucher, Ryan Henkensiefken, Gaurav Sant, and Jason Weiss. Shrinkage mitigation strategies in cementitious systems: A closer look at differences in sealed and unsealed behavior. *Transportation Research Record: Journal of the Transportation Research Board*, 2070(1):59–67, 2008.
- [64] Khossrow Babaei and Ronald L Purvis. Prevention of cracks in concrete bridge decks: Report on laboratory investigations of concrete shrinkage. Technical report, 1995.
- [65] Frank Collins and JG Sanjayan. Effect of pore size distribution on drying shrinking of alkali-activated slag concrete. *Cement and Concrete Research*, 30(9):1401–1406, 2000.
- [66] Frank Collins and JG Sanjayan. Cracking tendency of alkali-activated slag concrete subjected to restrained shrinkage. *Cement and Concrete Research*, 30(5):791–798, 2000.
- [67] Frank Collins and JG Sanjayan. Strength and shrinkage properties of alkali-activated slag concrete placed into a large column. *Cement and concrete research*, 29(5):659–666, 1999.
- [68] Frank Collins and Jay G. Sanjayan. Strength and shrinkage properties of alkali-activated slag concrete containing porous coarse aggregate. *Cement and Concrete Research*, 29(4):607 – 610, 1999.
- [69] M Palacios and F Puertas. Effect of superplasticizer and shrinkage-reducing admixtures on alkali-activated slag pastes and mortars. *Cement and Concrete Research*, 35(7):1358–1367, 2005.
- [70] M Palacios and F Puertas. Effect of shrinkage-reducing admixtures on the properties of alkali-activated slag mortars and pastes. *Cement and concrete research*, 37(5):691–702, 2007.
- [71] Monita Olivia and Hamid Nikraz. Properties of fly ash geopolymer concrete designed by taguchi method. *Materials & Design*, 36:191–198, 2012.
- [72] Steven H Kosmatka, William C Panarese, Gerald E Allen, and Stanley Cumming. *Design and control of concrete mixtures*, volume 5420. Portland Cement Association Skokie, IL, 2002.
- [73] Harrison Frederick Gonnerman. Tests of concrete containing air-entraining portland cements or air-entraining materials added to batch at mixer. In *ACI Journal Proceedings*, volume 40. ACI, 1944.
- [74] Paul Klieger. Studies of the effect of entrained air on the strength and durability of concrete made with various maximum sizes of sizes of aggregate. In *Highway Research Board Proceedings*, 1952.

A Appendix I: Mixture Proportion Information

Table 7: AAS mixture proportions for the determination of the effect of solution-binder ratio on compressive strength: § 3.1.2.

s/b	Na ₂ O %	M _s	AEA %	Coarse kg/m ³	Fine kg/m ³	Slag kg/m ³	H ₂ O kg/m ³	Na ₂ O kg/m ³	SiO ₂ kg/m ³	fw/b
0.40	2.5	1.5	0	780.0	713.4	570.0	192.37	14.25	21.38	0.34
0.40	2.5	2.5	0	780.0	713.4	570.0	178.12	14.25	35.63	0.31
0.40	2.5	3.5	0	780.0	713.4	570.0	163.87	14.25	49.88	0.29
0.40	3.37	2.5	0	780.0	713.4	570.0	160.77	19.21	48.02	0.28
0.45	2.5	1.5	0	780.0	773.9	506.7	196.32	12.67	19.01	0.39
0.45	2.5	2.5	0	780.0	773.9	506.7	183.65	12.67	31.68	0.36
0.45	2.5	3.5	0	780.0	773.9	506.7	170.98	12.67	44.35	0.34
0.45	3.37	2.5	0	780.0	773.9	506.7	168.23	17.08	42.69	0.33
0.50	2.5	1.5	0	780.0	822.3	456.0	199.35	11.40	17.25	0.44
0.50	2.5	2.5	0	780.0	822.3	456.0	188.10	11.40	28.50	0.41
0.50	2.5	3.5	0	780.0	822.3	456.0	176.70	11.40	39.90	0.39
0.50	3.37	2.5	0	780.0	822.3	456.0	174.21	15.37	38.42	0.38
0.55	2.5	1.5	0	780.0	861.9	414.5	202.10	10.36	15.54	0.49
0.55	2.5	2.5	0	780.0	861.9	414.5	191.74	10.36	25.90	0.46
0.55	2.5	3.5	0	780.0	861.9	414.5	181.37	10.36	36.27	0.44

Table 8: AAS mixture proportions for the determination of the effect of air entrainment on compressive strength: § 3.1.3.

s/b	Na ₂ O %	M _s	AEA %	Coarse kg/m ³	Fine kg/m ³	Slag kg/m ³	H ₂ O kg/m ³	Na ₂ O kg/m ³	SiO ₂ kg/m ³	fw/b
0.40	2.5	2.5	0.0	780.0	713.4	570.0	178.12	14.25	35.63	0.31
0.40	2.5	2.5	0.1	780.0	713.4	570.0	178.12	14.25	35.63	0.31
0.40	2.5	2.5	0.3	780.0	713.4	570.0	178.12	14.25	35.63	0.31
0.40	2.5	2.5	0.5	780.0	713.4	570.0	178.12	14.25	35.63	0.31
0.45	2.5	2.5	0.0	780.0	773.9	506.7	183.65	12.67	31.68	0.36
0.45	2.5	2.5	0.1	780.0	773.9	506.7	183.65	12.67	31.68	0.36
0.45	2.5	2.5	0.3	780.0	773.9	506.7	183.65	12.67	31.68	0.36
0.45	2.5	2.5	0.5	780.0	773.9	506.7	183.65	12.67	31.68	0.36
0.50	2.5	2.5	0.0	780.0	822.3	456.0	188.10	11.40	28.50	0.41

0.50	2.5	2.5	0.1	780.0	822.3	456.0	188.10	11.40	28.50	0.41
0.50	2.5	2.5	0.3	780.0	822.3	456.0	188.10	11.40	28.50	0.41
0.50	2.5	2.5	0.5	780.0	822.3	456.0	188.10	11.40	28.50	0.41

Table 9: AAF mixture proportion for determination of curing temperature effect on compressive strength: § 3.1.4.

s/b	Na ₂ O %	M _s	AEA %	Coarse kg/m ³	Fine kg/m ³	Fly Ash kg/m ³	H ₂ O kg/m ³	Na ₂ O kg/m ³	SiO ₂ kg/m ³	fw/b
0.45	2.5	2.5	0.1	780	673.1	506.7	183.66	12.67	31.67	0.36

Table 10: AAF mixture proportion for evaluation ambient temperature compressive strength development: § 3.1.4.

s/b	Na ₂ O %	M _s	AEA %	Coarse kg/m ³	Fine kg/m ³	Fly Ash kg/m ³	H ₂ O kg/m ³	Na ₂ O kg/m ³	SiO ₂ kg/m ³	fw/b
0.40	6.0	1.0	0.1	780	638.7	570	159.6	34.20	34.20	0.28

Table 11: AAS mixture proportion for evaluation ambient temperature compressive strength development: § 3.1.4.

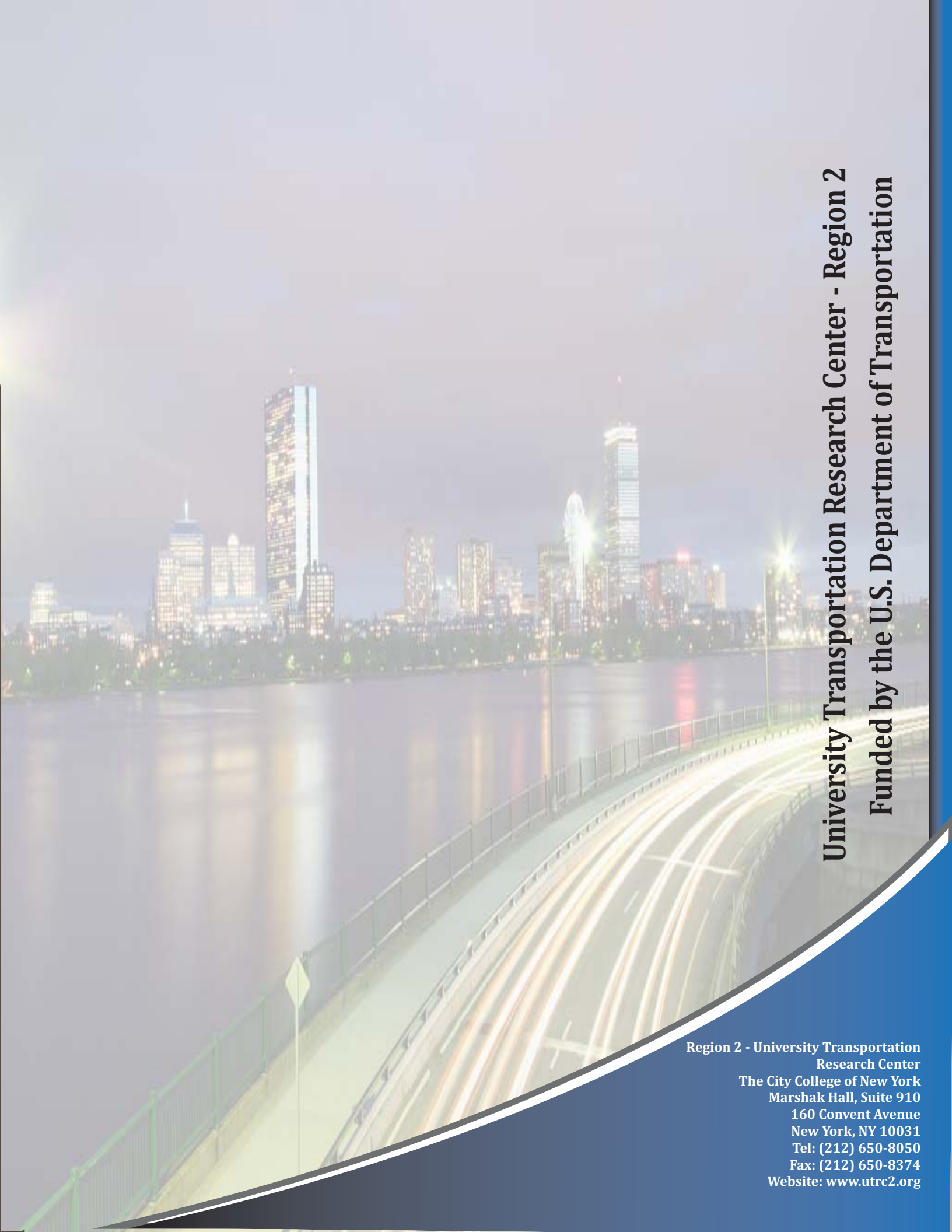
s/b	Na ₂ O %	M _s	AEA %	Coarse kg/m ³	Fine kg/m ³	Slag kg/m ³	H ₂ O kg/m ³	Na ₂ O kg/m ³	SiO ₂ kg/m ³	fw/b
0.40	5.0	0.75	0.1	780	713.4	570	178.12	28.5	21.38	0.31

Table 12: AAS mixture proportions for the determination of solution concentration effect on compressive strength: § 3.1.5-1.

s/b	Na ₂ O %	M _s	AEA %	Coarse kg/m ³	Fine kg/m ³	Slag kg/m ³	H ₂ O kg/m ³	Na ₂ O kg/m ³	SiO ₂ kg/m ³	fw/b
0.40	0.5	0.0	0.1	780	713.4	570	225.15	2.85	0.0	0.40
0.40	1.0	0.0	0.1	780	713.4	570	222.30	5.70	0.0	0.39
0.40	1.5	0.0	0.1	780	713.4	570	219.45	8.55	0.0	0.39
0.40	3.0	0.0	0.1	780	713.4	570	210.90	17.10	0.0	0.37
0.40	4.0	0.0	0.1	780	713.4	570	205.20	22.80	0.0	0.36
0.40	5.0	0.0	0.1	780	713.4	570	199.50	28.50	0.0	0.35
0.40	6.0	0.0	0.1	780	713.4	570	193.80	34.20	0.0	0.34
0.40	0.5	0.5	0.1	780	713.4	570	223.72	2.85	1.43	0.39
0.40	1.0	0.5	0.1	780	713.4	570	219.45	5.70	2.85	0.39
0.40	1.5	0.5	0.1	780	713.4	570	215.17	8.55	4.28	0.38
0.40	2.0	0.5	0.1	780	713.4	570	210.90	11.40	5.70	0.37
0.40	3.0	0.5	0.1	780	713.4	570	202.35	17.10	8.55	0.36
0.40	4.0	0.5	0.1	780	713.4	570	193.80	22.80	11.40	0.34
0.40	5.0	0.5	0.1	780	713.4	570	185.25	28.50	14.25	0.33
0.40	6.0	0.5	0.1	780	713.4	570	176.70	34.20	17.10	0.31
0.40	0.5	0.75	0.1	780	713.4	570	223.01	2.85	2.14	0.39
0.40	1.0	0.75	0.1	780	713.4	570	218.02	5.70	4.28	0.38
0.40	1.5	0.75	0.1	780	713.4	570	213.04	8.55	6.41	0.37
0.40	2.0	0.75	0.1	780	713.4	570	208.05	11.40	8.55	0.37
0.40	3.0	0.75	0.1	780	713.4	570	198.07	17.10	12.83	0.35
0.40	4.0	0.75	0.1	780	713.4	570	188.10	22.80	17.10	0.33
0.40	5.0	0.75	0.1	780	713.4	570	178.12	28.50	21.38	0.31
0.40	6.0	0.75	0.1	780	713.4	570	168.15	34.20	25.65	0.30
0.40	0.5	1.5	0.1	780	713.4	570	220.87	2.85	4.28	0.39
0.40	1.0	1.5	0.1	780	713.4	570	213.75	5.70	8.55	0.38
0.40	1.5	1.5	0.1	780	713.4	570	206.62	8.55	12.83	0.36
0.40	2.0	1.5	0.1	780	713.4	570	199.50	11.40	17.10	0.35
0.40	3.0	1.5	0.1	780	713.4	570	185.25	17.10	25.65	0.33
0.40	4.0	1.5	0.1	780	713.4	570	171.00	22.80	34.20	0.30
0.40	5.0	1.5	0.1	780	713.4	570	156.75	28.50	42.75	0.28
0.40	6.0	1.5	0.1	780	713.4	570	142.50	34.20	51.30	0.25
0.40	0.5	2.5	0.1	780	713.4	570	218.02	2.85	7.13	0.38
0.40	1.0	2.5	0.1	780	713.4	570	208.05	5.70	14.25	0.37
0.40	1.5	2.5	0.1	780	713.4	570	198.07	8.55	21.38	0.35
0.40	2.0	2.5	0.1	780	713.4	570	188.10	11.40	28.50	0.33
0.40	3.0	2.5	0.1	780	713.4	570	168.15	17.10	42.75	0.30
0.40	4.0	2.5	0.1	780	713.4	570	148.20	22.80	57.00	0.26

Table 13: AAF mixture proportions for the determination of solution concentration effect on compressive strength: § 3.1.5-2.

s/b	Na ₂ O %	M _s	AEA %	Coarse kg/m ³	Fine kg/m ³	Slag kg/m ³	H ₂ O kg/m ³	Na ₂ O kg/m ³	SiO ₂ kg/m ³	fw/b
0.40	1.0	0.0	0.1	780	638.7	570	222.30	5.70	0.0	0.39
0.40	2.0	0.0	0.1	780	638.7	570	216.60	11.40	0.0	0.38
0.40	3.0	0.0	0.1	780	638.7	570	210.90	17.10	0.0	0.37
0.40	4.0	0.0	0.1	780	638.7	570	205.20	22.80	0.0	0.36
0.40	5.0	0.0	0.1	780	638.7	570	199.50	28.50	0.0	0.35
0.40	6.0	0.0	0.1	780	638.7	570	193.80	34.20	0.0	0.34
0.40	7.0	0.0	0.1	780	638.7	570	188.10	39.90	0.0	0.33
0.40	8.0	0.0	0.1	780	638.7	570	182.40	45.60	0.0	0.32
0.40	1.0	0.5	0.1	780	638.7	570	219.45	5.70	2.85	0.39
0.40	2.0	0.5	0.1	780	638.7	570	210.90	11.40	5.70	0.37
0.40	3.0	0.5	0.1	780	638.7	570	202.35	17.10	8.55	0.36
0.40	4.0	0.5	0.1	780	638.7	570	193.80	22.80	11.40	0.34
0.40	5.0	0.5	0.1	780	638.7	570	185.25	28.50	14.25	0.33
0.40	6.0	0.5	0.1	780	638.7	570	176.70	34.20	17.10	0.31
0.40	7.0	0.5	0.1	780	638.7	570	168.15	39.90	19.95	0.30
0.40	8.0	0.5	0.1	780	638.7	570	159.60	45.60	22.80	0.28
0.40	1.0	1.0	0.1	780	638.7	570	216.60	5.70	5.70	0.38
0.40	2.0	1.0	0.1	780	638.7	570	205.20	11.40	11.40	0.36
0.40	3.0	1.0	0.1	780	638.7	570	193.80	17.10	17.10	0.34
0.40	4.0	1.0	0.1	780	638.7	570	182.40	22.80	22.80	0.32
0.40	5.0	1.0	0.1	780	638.7	570	171.00	28.50	28.50	0.30
0.40	6.0	1.0	0.1	780	638.7	570	159.60	34.20	34.20	0.28
0.40	7.0	1.0	0.1	780	638.7	570	148.20	39.90	39.90	0.26
0.40	8.0	1.0	0.1	780	638.7	570	136.80	45.60	45.60	0.24
0.40	1.0	1.5	0.1	780	638.7	570	213.75	5.70	8.55	0.38
0.40	2.0	1.5	0.1	780	638.7	570	199.50	11.40	17.10	0.35
0.40	3.0	1.5	0.1	780	638.7	570	185.25	17.10	25.65	0.33
0.40	4.0	1.5	0.1	780	638.7	570	171.00	22.80	34.20	0.30
0.40	5.0	1.5	0.1	780	638.7	570	156.75	28.50	42.75	0.28
0.40	6.0	1.5	0.1	780	638.7	570	142.50	34.50	51.30	0.25
0.40	1.0	2.0	0.1	780	638.7	570	210.90	5.70	11.40	0.37
0.40	2.0	2.0	0.1	780	638.7	570	193.80	11.40	22.80	0.34
0.40	3.0	2.0	0.1	780	638.7	570	176.70	17.10	34.20	0.31
0.40	4.0	2.0	0.1	780	638.7	570	159.60	22.80	45.60	0.28
0.40	5.0	2.0	0.1	780	638.7	570	142.50	28.50	57.00	0.25

A long-exposure photograph of a city skyline at night, reflected in a body of water. In the foreground, a bridge or highway has light trails from moving vehicles. The sky is dark, and the city lights are bright and colorful.

University Transportation Research Center - Region 2
Funded by the U.S. Department of Transportation

**Region 2 - University Transportation
Research Center**
The City College of New York
Marshak Hall, Suite 910
160 Convent Avenue
New York, NY 10031
Tel: (212) 650-8050
Fax: (212) 650-8374
Website: www.utrc2.org